NAVAL POSTGRADUATE SCHOOL
Monterey, California

THESIS

AN EXPERIMENTAL INVESTIGATION INTO THE FOREBODY AND ENGINE INLET AIRFLOW CHARACTERISTICS OF A PHOTOGRAPHIC RECONNAISSANCE WINDOW PALLET ON THE RF/A-18 AIRCRAFT

by

Joseph William Poole

June 1983

Thesis Advisor: Harvey W. Burden

SECURITY CLASSIFICATION OF THIS PAGE (When Data Entered)

REPORT DOCUMENTATION PAGE

READ INSTRUCTIONS BEFORE COMPLETING FORM

1. REPORT NUMBER

2. GOVT ACCESSION NO.

3. RECIPIENT'S CATALOG NUMBER

4. TITLE (and Subtitle)
An Experimental Investigation into the Forebody and Engine Inlet Airflow Characteristics of a Photographic Reconnaissance Window Pallet on the RF/A-18 Aircraft

5. TYPE OF REPORT & PERIOD COVERED
Master's Thesis
June 1983

6. PERFORMING ORG. REPORT NUMBER

7. AUTHOR(s)
Joseph William Poole

8. CONTRACT OR GRANT NUMBER(s)

9. PERFORMING ORGANIZATION NAME AND ADDRESS
Naval Postgraduate School
Monterey, Ca 93940

10. PROGRAM ELEMENT, PROJECT, TASK AREA & WORK UNIT NUMBERS

11. CONTROLLING OFFICE NAME AND ADDRESS
Naval Postgraduate School
Monterey, Ca 93940

12. REPORT DATE
June 1983

13. NUMBER OF PAGES
87

14. MONITORING AGENCY NAME & ADDRESS(if different from Controlling Office)

15. SECURITY CLASS. (of this report)
Unclassified

15a. DECLASSIFICATION/DOWNGRADING SCHEDULE

16. DISTRIBUTION STATEMENT (of this Report)
Approved for public release; distribution unlimited.

17. DISTRIBUTION STATEMENT (of the abstract entered in Block 20, if different from Report)

18. SUPPLEMENTARY NOTES

19. KEY WORDS (Continue on reverse side if necessary and identify by block number)
RF/A-18 , Reconnaissance Window Pallet , Moldline Change

20. ABSTRACT (Continue on reverse side if necessary and identify by block number)
A 1/7 scale model of a Navy F/A-18 forebody was built and tested in the Naval Postgraduate School Aeronautics Department Windtunnel to determine and measure the airflow total pressure distribution at the two engine inlet faces. The lower nose of this scaled model was then modified to incorporate a photographic reconnaissance window pallet, capable of holding two camera sensors within the existing gun bay. The model was retested using the same pressure measurement parameters and compared with the

DD FORM 1 JAN 73 1473 EDITION OF 1 NOV 65 IS OBSOLETE

S/N 0102-LF-014-6601

SECURITY CLASSIFICATION OF THIS PAGE (When Data Entered)

base aircraft test run to determine the airflow changes entering the engine inlets caused by this nose modification. Tufting was used on the model in each case to facilitate flow visualization observations and photography. The results of this investigation show that the pallet design tested caused no change in the airflow entering the engine intake ducts at low aircraft airspeeds.

Approved for public release; distribution unlimited.

An Experimental Investigation into the Forebody and Engine Inlet Airflow Characteristics of a Photographic Reconnaissance Window Pallet on the RF/A-18 Aircraft

by

Joseph William Poole
Lieutenant, United States Navy
B. S., Bowling Green State University, 1975
M. A., Webster College, 1977

Submitted in partial fullfillment of the requirements for the degree of

MASTER OF SCIENCE IN AERONAUTICAL ENGINEERING

from the

NAVAL POSTGRADUATE SCHOOL
June 1983

ABSTRACT

A 1/7 scale model of a Navy F/A-18 forebody was built and tested in the Naval Postgraduate School Aeronautics Department Windtunnel to determine and measure the airflow total pressure distribution at the two engine inlet faces. The lower nose of this scaled model was then modified to incorporate a photographic reconnaissance window pallet, capable of holding two camera sensors within the existing gun bay. The model was retested using the same pressure measurement parameters and compared with the base aircraft test run to determine the airflow changes entering the engine inlets caused by this nose modification. Tufting was used on the model in each case to facilitate flow visualization observations and photography. The results of this investigation show that the pallet design tested caused no change in the airflow entering the engine intake ducts at low aircraft airspeeds.

TABLE OF CONTENTS

LIST OF FIGURES

I. INTRODUCTION

A. BACKGROUND

For many years, the need for and importance of a tactical photographic reconnaissance aircraft has been well known to aviation operational commanders throughout the Navy. Since the decommissioning of the RF-8G Crusader Aircraft in 1981, this photographic reconnaissance mission has been fulfilled by the F-14 TARPS (Tactical Air Reconnaissance Pod System) program. This system incorporates an F-14 fuselage-mounted, streamlined window pod with camera sensors installed in it's interior. The TARPS program is a satisfactory interim solution to the Navy's reconnaissance requirements until a long term photographic reconnaissance platform is developed for Naval Aviation use.

The Navy's new F/A-18 Hornet is a prime candidate to fulfill these future photographic reconnaissance needs of the Navy. Detailed design studies to determine an RF/A-18 configuration compatible with the Navy's reconnaissance requirements have been in process for several year's at both the McDonnell-Douglas Aircraft Company (MCAIR) and at the Naval Air Development Center (NADC). MCAIR is the prime contractor for the F/A-18 Aircraft with headquarters in St. Louis, Missouri, and NADC is a Naval Research Field Laboratory in Warminster, Pennsylvania. One of the most promising designs resulting from these studies consists of the installation of two camera sensor stations in the F/A-18 nose and the incorporation of optical and/or infrared windows into the lower moldline [Ref. 1]. An investigation into the airflow characteristics of this design was the goal of this report.

B. PURPOSE OF THIS INVESTIGATION

Any modification to the existing F/A-18 Aircraft structure could have a possible impact on the propulsion/aerodynamic performance of the aircraft [Ref. 2]. One such possible impact could be the altering of the mass flow rate and total pressure distribution of air into the two engine inlets.

The purpose of this investigation was to determine if the proposed nose modification would change or alter the amount and distribution of air flowing through the engine inlet face. To this end, a 14.2% scaled forebody model of the F/A-18 was built and tested in the Naval Postgraduate School Aeronautical Engineering Department Windtunnel. The reconnaissance design modification was then incorporated on to the nose of the model and retested. Measurements of the engine airflow in each case were taken and compared to determine if any airflow change existed.

II. NATURE OF THE PROBLEM

A. BACKGROUND

The F/A-18 currently in production by MCAIR is capable of performing both the Fighter and Attack missions of the United States Navy. In order to additionally perform the photographic reconnaissance mission, camera sensors must be installed on or in the aircraft. These camera sensors would require viewing windows for target coverage.

The gun bay located on the F/A-18 nose barrel offers a ready-made, though not quite large enough cavity in which to mount camera sensors when the gun is removed (Fig. 1). To gain the additional space needed and to provide the necessary viewing windows, a modification to the existing structure of the F/A-18 nose lower moldline is required [Ref. 3]. The major factors which influence this lower moldline configuration are:

1. Camera sensor physical size and shape.
2. Camera sensor lateral viewing and window requirements.
3. Moldline contour effects on propulsion (engine inlets) and aerodynamics.

B. RECONNAISSANCE SENSORS IMPACT ON NOSE GEOMETRY

The reconnaissance camera sensor complement for the RF/A-18 was determined from mission capability requirements to be [Ref. 4]:

1. AAD-5 infrared reconnaissance set
2. KA-78 low altitude panoramic camera
3. KA-99 medium altitude panoramic camera
4. KA-100 high altitude panoramic camera
5. KS-127E Stand -off camera

It was also determined that two sensor stations were required to provide the necessary mission related sensor combinations. The sensors used to establish the volumetric and optical requirements for the RF/A-18 were the KS-127 stand-off camera and the KA-99/100 medium and high altitude panoramic cameras. These were chosen because they are the largest of the necessary sensors with the KS-127 camera being 56.5 inches in height and the KA-99/100 being 3.3 inches in height [Ref. 5] The physical size and shape of these cameras were found to slightly exceed the volumetric height of the existing gun bay by 2 inches, which was the driving force in determining the need for a lower nose moldline drop of 3 inches. A design capable of holding these two cameras will hold any combination of the five sensors.

The installation of two sensor stations in the F/A-18 nose also requires the incorporation of optical and/or infrared windows. Panoramic camera requirements dictate inclusion of side and lower windows for target viewing coverage. Many segmented window arrangements and moldline shapes have been evaluated by MCAIR in recent years [Ref. 6]. These have ranged from a simple two segment "V" to a six segment arrangement closely following the original fuselage contours. The design selected for investigation in this report (Fig. 2) was a promising configuration which included two sensor stations in the nose, two three segment sensor windows, lower moldline of nose dropped 3 inches, bottom flat on nose 11.2 inches wide, aircraft nose length unchanged, and side window flat angles of 54 degrees. The following sections discuss the rationale that determined the lower moldline contour.

1. Window and Camera Requirements

The photographic requirements for the RF/A-18 dictate the use of multiple sensors with varying characteristics [Ref. 7]. Sensors that provide imagery from the vertical to near horizontal plane are needed for downlooking and sidelooking photographic coverage. A camera system which includes a short focal length and small aperture lens will provide this capability and achieve acceptable resolution, with a resonable image scale, at low altitude. Systems with longer focal lengths and larger apertures are needed for the medium and high altitude portions of the flight envelope. The resolution and minimum range requirements for standoff coverage requires a system with a lens of even larger focal length and aperture size that can be pointed to various side depression angles, including those near the horizontal. A segmented window assembly with large side window panes is required to achieve these coverage capabilities (Fig. 3). These side windows must be coupled with a window assembly in the bottom of the sensor bay used for vertical photography.

The quality of sensor imagery is affected in several ways by the different characteristics of its window. Bright light rays have a high probability of entering the side panes and reflecting from the other panes into the field of view of the lens. This reflective effect is largest when the side panes are at a steep angle (Fig. 4). Contoured windows can deform the optical wavefront entering the lens aperture thereby requiring the use of flat windows. Photographs taken through seams on the window frame can block out portions of the image. Photographs taken through the seam separating the side and bottom window panes can cause an optical phase difference and angular error in the photographs because of the difference in optical path length (Fig. 5).

The impact of these effects on photo imaging depends on the geometric relationship between the camera lens aperture size and pointing angle, and the window characteristics such as glass thickness, seam thickness, and edge mating angles. Therefore, the photo image loss can be minimized for a specific sensor by optimizing the seam location, angle between the window panes, aperture size, and sensor installed location. The design window pallet studied in this report is a general configuration and arrangement considered to have optimized all of the aforementioned characteristics.

C. NOSE GEOMETRY IMPACT ON PROPULSION/AERODYNAMICS

1. Propulsion Compatibility

The impact of nose contour on the propulsion performance of the aircraft was the major design factor considered in this investigation. Smooth, trouble-free engine operation requires that certain total pressure levels of air be supplied to the engine face. Quality inlet flowfields are obtained through good boundary layer control and minimal total pressure distortion level along the forebody of the aircraft. Total pressure distortion is a measure of the deviation from uniform, constant total pressure airflow. Premature boundary layer separation and/or excessive inlet flowfield distortion levels degrade the quality of air entering the inlets and hinders smooth engine operation.

The nose geometry design of the F/A-18 production aircraft must be such that adequate total pressure levels of air enter the F404-GE-400 turbofan engine inlets throughout the aircraft's entire flight regime. Selection of a suitable reconnaissance nose contour is therefore dictated

by the need to supply this same adequate flowfield into the engine inlets.

By properly utilizing the testing capabilities of the Naval Postgrauduate School Aeronautics Department Windtunnel, accurate measurements of the total air pressure entering the engine inlets of a model aircraft could be made. A scaled replica of the baseline production F/A-18 aircraft forebody was constructed, tested and then modified with the subject reconnaissance window pallet and retested. Comparison of the two tests can be used to gain a general insight into the magnitude of the effects of the design modification on the total pressure distribution at the engine inlet faces.

2. Aerodynamic-Optical Considerations

Minimizing the reconnaissance window pallet's deviation from the basic nose barrel shape is desirable from the standpoint of local flowfield properties as well as aerodynamic drag and stability considerations. On a reconnaissance modified F/A-18, a recompression shock wave is expected to be generated on the forward portion of the window pallet at Mach numbers of around .8 and higher [Ref. 8]. Such a shock would occur on any flat plate area due to a tendency towards a supersonic expansion around the leading edge of the flat plate area (Fig. 6). However, minimizing the depth of the window pallet will minimize the shock strength. This would provide the least possible distortion in the local airflow field through which the camera sensors must look.

To insure good aero optical qualities in the flowfield surrounding the sensor windows, the reconnaissance pallet blends a smoothly sloping forward window ramp into the existing nose barrel. This minimizes the effect of the flat plate area on flow field distortion by producing

a weaker shock. This forward window ramp can also act as a forward looking camera port.

III. EQUIPMENT

A. WINDTUNNEL

The wind tunnel at the Naval Postgraduate School used for this testing program is a West Coast Research Company built, vertical, closed circuit, single return wind tunnel with an octagonal, closed jet test section [Ref. 9]. The test section is 3.5 feet high by 5.0 feet wide by 8.0 feet long. The overall dimensions of the entire wind tunnel are 11.5 feet X 38 feet X 65.5 feet (Fig's 7,8).

The power section of the tunnel comprises a 150 horsepower electric motor coupled to a four bladed variable pitch fan by a constant speed Curtis Wright transmission.

Directly downstream of the fan is located a set of 4 stator blades, commonly called the flow straightener. The flow straightener removes the twist imported by the fan thus reducing the losses and turbulence which would otherwise occur.

Turning vanes are used in the bend at the first and each corner of the tunnel in order to turn the flow of air. Additionally they minimize the loss of kinetic energy of the air due to turning which would manifest itself as a loss in pressure. These vanes are precisely oriented so that air flow separation does not occur at the leading edges.

The air continues flowing through the ducting, a large portion of which is used to diffuse the air. The return passage serves this purpose

in addition to completing the circuit and ultimately returning the air to the test section.

The flow continues through two more sets of turning vanes at the corners and then into the settling chamber. Here, the cross sectional area of the tunnel is the greatest, hence the velocity is the least. The larger the cross sectional area of the settling chamber compared with that of the test section, the greater will be the probability of low turbulence in the test section. This tunnel has a 7 to 1 settling chamber to test section ratio.

After the settling chamber, the air flows into the contraction cone whose principle function is to accelerate the low speed air to the velocity required in the test section. In addition, because of its continually decreasing cross section, the contraction cone tends to produce a more uniform distribution of velocity in the test section.

The air then flows into the test section which is of octogonal design. Each side of the test section consists of hinged doors upon which plate glass windows are installed. This permits easy access into the tunnel and unobstructed viewing of the test model during tunnel operation. This test section, like that of most low speed tunnels, operates at atmospheric pressure. Since the air flow velocity is greatest here, the pressure is lowest, which means that the pressure everywhere else in the circuit is above atmospheric. Consequently, some leakage will occur through the duct walls since it is virtually impossible to make the tunnel airtight. If nothing were done to correct for this, the pressure in the test section would drop below atmospheric, resulting in leakage into the tunnel at this critical point. For this reason a breather slot

is installed immediately downstream of the test section. This slot, 1 inch wide and extending the full length of each side, allows air to flow into the circuit to make up leakage losses and insures that the test section remains at a uniform pressure.

The diffuser of the tunnel is a gradually widening duct downstream of the test section, providing for the efficient conversion of the kinetic energy of the air into pressure energy. Thus it serves to prevent excessive friction losses due to high flow velocities. Although most of the ducting in the tunnel serves to diffuse the air, the term "diffuser" is commonly applied only to that part of the circuit situated between the test section and the first corner. Within the diffuser of this windtunnel are four splitter vanes to help direct and straighten the flow. Also in this diffuser is a protective screen constructed of heavy wire. The sole purpose and function of this screen is to protect the turning vanes and fan from damage should there be a model or mount failure.

Located on the wall of the settling chamber is a temperature gauge which is connected to a thermocouple extending into the tunnel. This gauge indicates the local temperature in the settling chamber in degrees Fahrenheit.

Static pressure taps are placed at two sections of the wind tunnel sufficiently far forward of the test section so that pressure changes induced by the model are negligible. There are 4 static piezometer taps, situated 1 on each wall, at a section of the settling chamber just downstream of the turning vanes and 4 more at a section in the contraction cone near the test section.

This windtunnel operates with the test section static pressure at local ambient and has a maximum velocity of 175 Knots. The tunnel turbulence factor is 1.35.

B. MODEL

The size, construction, and dimensions of this 14.2% model (Fig's 9-20) were dictated by the wind tunnel in which it was to be tested. Since all data desired concerned the lower front portion of the aircraft, only the forward half of the aircraft was modeled and constructed. This allowed the highest Reynolds number possible for testing in the 3.5 foot X 5 foot test section. The model Reynolds number based on wing root cord is 3.5 million.

The model was constructed of Jelutong wood, a medium hard wood used frequently by professional model builders because of its hardness qualities, workability and maintainability. Scaled drawings were made with dimensions taken from the F/A-18 Aircraft Weight and Balance Manual. These drawings were then used as male templates by the model builder to construct the model.

A black pigmented lacquer was used as a finish on the model because of its smoothness qualities. Four coats were applied and sanded using progressively finer waterproof sandpaper.

The model was assembled on a plate mount of the same type to be used in the wind tunnel test section. Since the bottom of the aircraft was to be the area considered for testing, the model was built to be attached to the test section floor mount upside down. This allowed for uninterrupted

airflow along the belly. The mount was centered and fastened through the top portion of the aircraft.

1 3/4 inch tufts of white 2-ply cotton thread were used as the flow visualization apparatus for this experiment. A tufting board was used to attach the tufts at 1 inch intervals along strips of 3/4 inch Scotch transparent cellophane tape. These tufting strips were then applied to the model at 3 inch intervals along the entire length of the model.

C. RECONNAISSANCE WINDOW PALLET

The window pallet was constructed of standard professional modelling clay and was built directly on the model aircraft (Fig. 21). It too was a 14.2% scaled replica of the pallet being considered by MCAIR and NADC for the RF/A-18 Aircraft. The contour of the pallet and its effect on the airflow of the aircraft's forebody and engine inlets are the subject of this report. The pallet's exterior dimensions were used to reproduce a duplicate, in scaled form, of the design modification consisting of a three inch lower moldline drop with a bottom window flat width of 11.2 inches and side window flats angled 54 degrees from the horizontal.

D. TURBULENCE SPHERE

To determine the Tunnel Turbulence Factor shown calculated in Appendix B, a 6 7/8 inch diameter turbulence sphere was used (Fig. 22). This sphere has 20 pressure taps located on its surface. These taps are connected, via 1/8 inch flexible plastic tubing, to a manometer board used in measuring pressure differences. One orifice is located at the forward

stagnation point. Four other orifices are located 22 1/2 degrees off the longitudinal axis near the rear of the sphere. These four taps are connected together to yield an average base pressure. The pressure difference is measured between the forward and rear taps of the sphere.

E. PITOT TUBE

To determine the Tunnel Calibration Factor shown calculated in Appendix A, a pitot static L-probe was used as the air data collector (Fig. 23). The opening in the front of the probe senses the stagnation pressure, while the small holes around the outer periphery of the tube sense the static pressure [Ref. 10]. This pitot tube was connected via 3/8 inch flexible tubing to a manometer board for pressure measurements.

F. INTAKE PRESSURE PROBES

Each engine inlet face of the 1/7 scale model was mounted with six basic total pressure probes constructed of 1/8 inch metal tubing (Fig. 24). In each instance the opening in the probe is oriented parallel to the air flow. These inlet pressure probes were connected via 1/8 inch flexible plastic tubing to a manometer board and measured total pressure.

G. MANOMETER BOARD

A well-type manometer board scaled in inches and containing colored water was used in this investigation to measure all pressure data (Fig. 25). A water reservoir mounted on the manometer board supplied each manometer tube with identical water levels at atmospheric pressure. Individual

water column's which were attached to pressure probes within the operating wind tunnel registered a displacement from the atmosphic pressure level. By measuring this displacement, pressure differentials were determined [Ref. 11].

IV. EXPERIMENTAL PROCEDURE

The airflow condtitions that exist in the Naval Postgraduate School Aeronautics Department Windtunnel were examined to determine the tunnel calibration and tunnel turbulence factors. A calibrated L-type pitot tube, placed in the center of the unobstructed test section, measured the actual dynamic pressure of the tunnel throughout it's speed range. A graph of the pressure differential across the contraction cone (Δp) versus test section dynamic pressure (q) was generated from these measurements (Fig. 26). The slope of the resulting curve determined the tunnel calibration factor..

Next, a turbulence sphere was placed in the test section. The airflow difference between the forward and rear pressures on the sphere were measured and then divided by the tunnel dynamic pressure and plotted against Reynolds number. Knowing experimentally that the drag coefficient of a sphere is 0.3 when $\Delta p/q$ is 1.22 [Ref. 12] allowed the calculation of the tunnel critical Reynolds number. The tunnel turbulence factor was then found by dividing the critical Reynolds number of turbulent free air [Ref. 13] by the tunnel's critical Reynolds number (Fig. 27).

After completing tunnel calibration, the 1/7 scale model was mounted into the test section. Wake and solid blockage calculations were

made, and the model tested at the tunnel's highest airflow speed of 175 knots. Engine inlet air pressure was measured within the model aircraft's angle of attack range of +15 degrees to -20 degrees by the use of pressure taps arranged on the inside perimeter of the inlet face (Fig. 24) and attached to a manometer board. The model was tufted and photographed to allow flow visualization observations. Upon completion of data collection a graph of the mean and standard deviation of total engine inlet pressure versus angle of attack was generated. Tunnel dynamic pressure versus angle of attack was also plotted.

Next, the photographic reconnaissance window pallet modification was built on the model and tufted. This modified model was put through the same test as the baseline model with measurements again recorded at a tunnel speed of 175 Knots and at an angle of attack range of +15 degrees to -20 degrees. Photograph's were also taken again for flow visualization comparisons (Fig.'s 28-33). Finally, graphs of tunnel dynamic pressure versus angle of attack, and of total engine inlet pressure versus angle of attack were plotted for comparison with the base aircraft model run. The goal of this procedure was to determine if the airflow entering the engine inlets was changed or diverted because of nose modification.

V. RESULTS

A. TUNNEL CALIBRATION

The tunnel calibration factor described in Appendix A is 1.0355 (Fig. 26). The tunnel turbulence factor shown calculated in Appendix B is 1.35 (Fig. 27).

B. BASELINE AND MODIFIED MODEL PRESSURE MEASUREMENTS

Engine inlet total pressure versus aircraft angle of attack results are graphed in Figure's 34 and 35 for both the baseline and modified model. Tunnel dynamic pressure versus aircraft angle of attack results for both models are graphed in Figure 36. Individual inlet pressure probe measurements are recorded in Figure's 37 and 38.

C. FLOW VISUALIZATION COMPARISONS

Characteristics of the airflow over the F/A-18 model and it's modified RF/A-18 variant can be visualized by observing the white tufts against the black model forebody. Photograph's of this at selected angle's of attack of +15°, +12°, 0°, -8°, -15°, and -20° are shown in Figure's 28 through 33.

D. CALCULATIONS

Tunnel calibration calculations can be found in Appendix A. Tunnel turbulence calculations can be found in Appendix B. All other formula's used and their results can be found in Appendix C.

VI. ANALYSIS

A. TUNNEL CALIBRATION

As described in detail in Appendix A, a tunnel calibration curve should be linear and is obtained by plotting Δp versus q_{true}. This tunnel calibration factor simply relates the test section velocity of any given wind tunnel to that of the free airstream. For the wind tunnel used in this investigation a very acceptable and linear calibration factor of 1.0355 was determined.

The tunnel turbulence factor discussed in Appendix B is dependent on the wind tunnel's design and construction. This factor changes slightly with tunnel speed but is nearly constant for each tunnel. Turbulence factors range from 1.0 to 3.0 with a value of less that 1.4 required to obtain good test results. The calculated tunnel turbulence factor of 1.35 for the windtunnel used in this experiment is therefore considered acceptable.

B. MODEL PRESSURE MEASUREMENTS

1. Total Engine Inlet Pressure vs. Angle of Attack

The six individual probes mounted on the perimeter of each engine inlet (Fig. 24) provided a measurement of the airflow pressure entering that inlet probe. The Mean and Standard Deviation of the 12 probe data measurements were calculated at each of the six selected angles of attack. The difference between atmospheric pressure and measure airflow pressure allowed the engine inlet pressure distribution to be determined. The

results of this(Fig's 34, 35) show a nearly exact duplication between the baseline aircraft engine inlet total pressure distribution and the reconnaissance modified aircraft inlet total pressure distribution.

Furthermore, a detailed study of Figures 37 and 38 shows a very close correspondence of the pressure distributions, at each individual inlet probe, between the baseline and modified aircraft test runs. This confirms the similarity of engine inlet total pressure distributions between these two aircraft models.

2. Tunnel Dynamic Pressure vs. Angle of Attack

The tunnel dynamic pressure, as measured by the piezometer taps in the contraction cone, give an indication of the tunnel velocity. Any obstruction in the test section will alter the dynamic pressure and hence the velocity. The dynamic pressure of the tunnel was measured and recorded during the baseline aircraft test runs. The same was accomplished throughout the modified aircraft runs. The results of these data recordings (Fig. 36), indicate that there was no change in velocity between the baseline and modified aircraft. Since the model tested had an excellent testing Reynolds number of 3.5×10^6, the data can be interperted to mean that the propose nose modification will have no effect on the F/A-18 Aircraft velocity in low speed flight.

C. FLOW VISUALIZATION COMPARISONS

No appreciable change in airflow over the forebody is observed between the baseline and modified aircraft at any of the angle's of attack photographed.

D. CALCULATIONS

A minimun testing Reynolds number of 1,500,00 to 2,500,00 is desired in any wind tunnel test program to insure accurate findings [Ref. 14]. Actually there is little need to have more than 2,500,000 unless about 9,000,000 is attained [Ref. 15]. The Reynolds number of 3,5000,000 for the test model used in this investigation is therefore considered excellent.

The presence of a model in a test section reduces the flow area, and hence by Bernoulli's principle increases the velocity of the air through the test section. This increase in velocity is called "solid blocking". Additionally, any model will have a wake behind it caused by the detachment of the model's boundary layer. This wake causes an increase in the velocity of air around it. The velocity increase here is called "wake blocking". "Total blockage " is the sum of the solid and wake blockage. In order to more closely correlate the airflow in the test section to that of the outside free airstream, a total blockage correction must be made to the test section measured velocity. A total blockage correction factor of .01928 was calculated and applied in this experiment.

E. ANOMALOUS BEHAVIOR

A noteworthy deviation in flow patterns occured during testing at an aircraft angle of attack setting of -15^{o} (Fig. 44). Here, a large decrease in pressure was recorded at the outside pressure probe of each inlet (Fig. 24). A clear cut reason for this occurrence is not known. However, a possible explaination was evaluated during test observations.

As the aircraft's angle of attack was decreased through the -12° and into the -15° range an increase in the vorticity of the flow was observed through use of tufts. It is believed that these flow vorticies were shed by the aircraft causing an excessive angular flow distortion from the centerline area of the aircraft outwards. This could prevent adequate pressure from reaching the probe. This occurrence was noted on both the baseline and modified aircraft, thereby not altering the comparison conclusions.

Possible causes of this vortex shedding could be, anomalies in test section airflow, model body coarseness resulting from the use of cellophane tape for tufting, or actual aircraft patterns.

VII. CONCLUSIONS AND RECOMMENDATIONS

Analysis of the results of this investigation show that there is no significant change in the engine inlet total pressure distribution. When a photographic reconnaissance window pallet of the design studied is incorporated on the lower nose moldline of the F/A-18 Aircraft (Fig.'s 34-35). Additionally, it was concluded that this nose modification does not alter the velocity of the aircraft in flight (Fig. 36). Both of these conclusions are applicable only to the low speed flight regime of 175 Knots or less.

The following recommendations are made:

1. The Naval Air Development Center should utilize the readily available bank of Aeronautical Engineering thesis students and the Naval Postgraduate School Aeronautics Department Windtunnel testing capabilities to pursue this and other aeronautics related research.

2. Further study and testing of the photographic reconnaissance window pallet lower moldline modification investigated in this report should be done. These tests could include local airflow angularity changes, total pressure distortion level measurements, flowfield measurements over a full RF/A-18 Aircraft model, effects of window pallet on sideslip, drag, lift, etc.

3. Windtunnel tests should be made with various size window pallet modifications. This could determine the maximum extent to which the nose lower moldline may deviate from the existing F/A-18 nose barrel shape before altering airflow characteristics. Larger reconnaissance

window pallets would benefit photo-imaging parameter such as viewing angles, number of sensor stations, and standoff range coverage.

APPENDIX A: TUNNEL CALIBRATION FACTOR

The conditions under which a model is windtunnel tested are not the same as those in free air. The important flow characteristics in a low speed windtunnel are it's airflow distribution of dynamic, static, and total pressures, and its temperature and turbulence [Ref. 16]. A "tunnel calibration factor" can be determined which will more closely relate tunnel airflow to free airstream flow. This calibration factor relates pressure differential measurements to test section velocity. Once the flow characteristics of the airstream are defined, the velocity and Reynolds number for a particular model may be computed. The following sections describe and determine the tunnel turbulence factor for the Naval Postgraduate School Aeronautics Department Windtunnel.

A. THEORETICAL

It is not practical to insert a pitot tube in the test section near a model. Its presence would interfere with the air flow around the model and lead to erroneous test results. Most wind tunnels resort to an indirect measurement of tunnel air speed. This is done by correlating the pressure change across the contraction cone to the velocity in the test section [Ref. 17].

To examine how the pressure change and velocity are related, the energy equation between the entrance to the contraction cone and the entrance to the test section must be written. Since the Naval Postgrad-

ate School Aeronautics Department 3.5 ft. X 5 ft. Windtunnel operates at relatively low speeds the equation for incompressible flow is valid (Fig. 39);

$$\frac{P_1}{\rho} + \frac{V_1^2}{2g_c} + \frac{g}{g_c} z_1 = \frac{P_2}{\rho} + \frac{V_2^2}{2g_c} + \frac{g}{g_c} z_2 + \omega_{s_{1-2}} + h_{f_{1-2}} \qquad \text{A-1}$$

Changes in potential are neglected and no shaft work is involved between stations 1 and 2. The last term, h_f, represents the losses in the contraction cone. By neglecting these losses, the ideal case is considered. Rearranging the terms of eq. A-1 gives the pressure change.

$$P_1 - P_2 = \frac{\rho}{2g_c}\left(V_2^2 - V_1^2\right) = \rho \frac{V_2^2}{2g_c}\left[1 - \frac{V_1^2}{V_2^2}\right] \qquad \text{A-2}$$

The continuity equation is now introduced;

$$\rho_1 A_1 V_1 = \rho_2 A_2 V_2 \qquad \text{A-3}$$

for ρ = constant

$$\frac{V_1}{V_2} = \frac{A_2}{A_1}$$

Substituting eq. A-3 into eq. A-1 enables a solution for the ideal velocity at section two to be given in terms of the pressure change across the contraction cone and the tunnel area ratio.

$$V_{2\,ideal} = \sqrt{\frac{2g_c \Delta P}{\rho\left(1 - (A_2/A_1)^2\right)}} \qquad \text{A-4}$$

This equation can also be squared and rearranged to obtain an expression for the dynamic pressure. The dynamic pressure in the test section is normally referred to as the tunnel "q". The ideal q is

directly related to the measured pressure difference (Δp) and tunnel geometry by

$$q_{ideal} = \frac{\rho V_{2\,ideal}^2}{2g_c} = \frac{\Delta P}{1-\left(\frac{A_2}{A_1}\right)^2} \qquad A\text{-}5$$

$$q_{ideal} = \text{constant}\,(P_1 - P_2) \qquad A\text{-}6$$

For most tunnels the square of the area ratio is negligible. Thus the constant indicated in eq. A-6 is approximately unity. Note that eq. A-6 represents the ideal tunnel q. The actual q will be slightly different due to the viscous and three-dimensional effects that were neglected in eq A-1. However, the expression indicates that the final calibration between Δp and q should essentially be linear.

B. EXPERIMENTAL

The actual tunnel q is measured with a calibrated pitot tube which is placed in the center of the test section. The difference between the total and static pressure indicated by the pitot tube directly represents the tunnel q.

$$P_{t_3} - P_3 = \frac{\rho V_3^2}{2g_c} = q_{true} \qquad A\text{-}7$$

Piezometer rings, which have taps on all four walls of the tunnel, enable average pressure to be detected at stations one and two. Thus, Δp and true q can be measured by two differential micromanometers. A calibration curve is obtained by plotting Δp versus q_{true}. In most cases this curve is linear and its slope is called the "tunnel calibration factor ".

C. CALCULATIONS

Δp_{1-2} (cm H_2O)	p_t (in. H_2O)	p_s (in. H_2O)	Δp (in. H_2O)	$\Delta p = q_t$ (cm H_2O)
10	10.25	14.07	3.82	9.703
20	6.65	14.28	7.63	19.38
30	3.23	14.52	11.29	28.68
35	1.35	14.65	13.3	33.78

Slope (Fig. 26) = $\Delta p/q$ = tunnel calibration factor = 1.0355

APPENDIX B: TUNNEL TURBULENCE FACTOR

A. DISCUSSION

If a sphere were tested in turbulent free air, the critical Reynolds number would be exactly 385,000 [Ref. 18]. The critical Reynolds number is the Reynolds number for which the coefficient of drag is equal to 0.3 [Ref. 19]. The turbulence factor for any particular tunnel can be calculated by

$$\text{turbulence factor} = \frac{385{,}000}{R_{crit}} \qquad \text{eq. B-1}$$

To determine the critical Reynolds number for the windtunnel used in this investigation the following procedures were employed:

1. A 6 7/8 inch diameter sphere was placed in the tunnel test section (Fig. 22). The pressure difference was measured and recorded between the forward and rear taps.

$$\Delta p = p_{forward} - p_{rear\ (avg)} \qquad \text{eq. B-2}$$

2. This Δp was then divided by the corrected tunnel dynamic pressure.

3. The Reynolds number based on diameter was calculated for the sphere.

4. A plot of $\Delta p/q$ versus Reynolds number was generated to determine the critical Reynolds number (Fig. 27). It has been found experimentally that when $\Delta p/q = 1.22$ the drag coefficient of the sphere is 0.3 [Ref. 12].

5. The tunnel turbulence factor was then calculated as indicated in eq. B-1.

B. CALCULATIONS

1. Sphere Pressure Measurements

$\Delta p_{1-2} = \Delta h$ (cm H_2O)	$p_{forward}$ (in. H_2O)	$p_{rear\ (avg)}$ (in. H_2O)	$\Delta p_{(forward-rear)}$ (in. H_2O)
3	12.49	10.8	1.69
4	12.12	10.32	1.80
5	11.96	10.00	1.96
6	11.90	9.98	1.92

2. Tunnel Dynamic Pressure Correction

The test section cross sectional area is (Fig. 8)

$$A_{xc} = 0.828\,(60\ in)(42\ in) = 2087\ in^2 \qquad B\text{-}3$$

The total blockage factor is

$$\frac{\Delta u}{u} = \frac{1}{4}\,\frac{\pi/4\,(6\tfrac{7}{8})^2}{A_{xc}} = 0.004448 \qquad B\text{-}4$$

The corrected velocity is

$$u_c = u_u + \frac{\Delta u}{u_u} u_u \qquad B\text{-}5$$

Substituting $\Delta u/u$ yields

$$u_c = 1.004448\, u_u \qquad B\text{-}6$$

The corrected dynamic pressure is given by

$$q_c = \tfrac{1}{2}\rho u_c^2 = \tfrac{1}{2}\rho (1.004448)^2 u_u^2 = (1.004448)^2 q_u \qquad B\text{-}7$$

The uncorrected dynamic pressure is

$$q_u = \frac{1}{0.971}\,\Delta h \qquad \text{B-8}$$

Substituting into eq. B-7

$$q_c = (1.00448)^2 \frac{1}{0.971}\,\Delta h \qquad \text{B-9}$$

$$q_c = 1.039\,\Delta h \qquad \text{B-10}$$

Dividing Δp by q_c

$$\frac{\Delta p}{q_c} = \frac{\Delta p\ (\text{in } H_2O)(2.54\ \text{cm/in})}{1.039\,\Delta h\ (\text{cm } H_2O)} \qquad \text{B-11}$$

$$\frac{\Delta p}{q_c} = 2.44\ \frac{\Delta p\ (\text{in } H_2O)}{\Delta h\ (\text{cm } H_2O)} \qquad \text{B-12}$$

3. Sphere Reynolds Number Based on Diameter

The Reynolds number is given by

$$R = \frac{\rho u l}{\mu} = \frac{\rho l}{\mu} u_c = \frac{\rho l}{\mu}\sqrt{2 q_c/\rho} \qquad \text{B-13}$$

$$R = \frac{l}{\mu}\sqrt{2\rho}\ \sqrt{1.039\,\Delta h} \qquad \text{B-14}$$

where

$l = d = 6.875/12$ ft B-15

$\mu = 3.82 \times 10^{-7}$ lb-sec/ft^2 B-16

$\rho = 0.00233$ lb-sec^2/ft^4 B-17

1 in = 2.54 cm B-18

Substituting eq.'s B-15 through B-18 into eq. B-14 yields

$$R_d = \frac{6.875/12}{3.82 \times 10^{-7}}\ \sqrt{2 \times 0.00233}\ \sqrt{1.039\,\Delta h\ (\text{cm } H_2O)}\ \frac{62.4\ \text{lb/ft}^3}{30.48\ \text{cm } H_2O} \qquad \text{B-19}$$

Reducing

$$R_d = 146{,}906\ \sqrt{\Delta h\ (\text{cm } H_2O)} \qquad \text{B-20}$$

4. Tabular Summary of Calculations

$\Delta h = \Delta P_{CONTRACTION\ CONE}$

$\Delta P = P_{FORWARD} - P_{REAR}$ B-2

$\frac{\Delta P}{q} = 244 \frac{\Delta P\ (in\ H_2O)}{\Delta h\ (cm\ H_2O)}$ B-12

$R_d = 146{,}906 \sqrt{\Delta h\ (cm\ H_2O)}$ B-20

$\frac{\Delta h}{(cm\ H_2O)}$	$\frac{\Delta p}{(in.\ H_2O)}$	$\Delta p/q_c$	R_d
3	1.69	1.370	254,448
4	1.80	1.098	293,812
5	1.96	0.957	328,492
6	1.92	0.781	359,845

5. Tunnel Turbulence Factor

The results of these $\Delta p/q_c$ and R_d calculations are shown on the graph of Fig. 27. From this graph, the critical Reynolds number is determined to be 285,000. Substituting this value into eq. B-1 yields a tunnel turbulence factor of 1.35.

APPENDIX C: FORMULA'S AND CALCULATIONS

The aircraft model total blockage factor is

$$\frac{\Delta u}{u} = \epsilon = \frac{1}{4}\,\frac{\text{MODEL X-C AREA}}{\text{TEST SECTION AREA}}$$

$$= \frac{1}{4}\,\frac{160.9\ \text{in.}}{(.828)(60\text{in} \times 42\text{in})} = 0.01928$$

The corrected tunnel dynamic pressure is given by

$$q_c = \tfrac{1}{2}\rho u_c^2 = K_1 q_u = K_1 K_2 \Delta h\ (\text{cm}\,H_2O)$$

where

$$K_1 = 1 + \epsilon = 1.01928$$

$$K_2 = \frac{1}{0.971}$$

The corrected test section velocity (ft/sec) in terms of the uncorrected velocity is

$$u_c = 1.01928\, u_u$$

$$u_c^2 = 1.039\, u_u^2$$

therefore

$$q_c = 1.039 q_u = 1039\left(\frac{1}{.971}\right)\Delta h\ (\text{cm}\,H_2O)$$

$$q_c = 1.070\,\Delta h$$

converting to lb/ft^2

$$q_c = 1.070\,\Delta h\,(\text{cm}\,H_2O)\ 2.047\ \frac{lb/ft^2}{\text{cm}\,H_2O}$$

We can now calculate the corrected tunnel velocity

$$u_c = \sqrt{2/\rho}\,(1.070)(2.047)\ \sqrt{\Delta h\ (\text{cm}\,H_2O)}$$

$$= \sqrt{2/.0023\,(1070)(2.047)}\ \sqrt{44} = 289.5\ ft/SEC$$

Converting to Knots yields

$$u_c = 289.5\left(\frac{60}{88}\right)\left(\frac{5280}{6000}\right) = 173.7\ \text{knots}$$

The model Reynolds number based on root chord can now be calculated.

$$R_c = 599{,}030\ \sqrt{\Delta h\ (\text{cm}\,H_2O)}$$

$$= 599{,}030\ \sqrt{35.25}$$

$$= 3{,}556{,}540$$

APPENDIX D: WINDTUNNEL OPERATING PROCEDURES

The following procedures apply to the Naval Postgraduate School Aeronautical Engineering Department 3.5 ft. X 5.0 ft. Windtunnel.

1. Ensure windtunnel and test section are clear of all personnel and obstruction (Fig. 40).

2. Turn switch on power panel (Fig. 41) to the 220 V position.

3. Decrease propeller pitch fully by use of the two toggle switches on the control panel (Fig. 42).

4. Press the start button on the control panel.

5. Increase propeller pitch by use of toggle switches on control panel until the desired tunnel speed and/or tunnel pressure is reached. The pressure differential (Δp) across the contraction cone can be read by use of the U-tube manometer (Fig. 43) next to the control panel.

6. When tunnel operation is complete, decrease the propeller pitch fully by use of the toggle switches on the control panel.

7. When prop pitch is fully decreased, push stop button.

8. Turn 220 V switch on power panel to the off position.

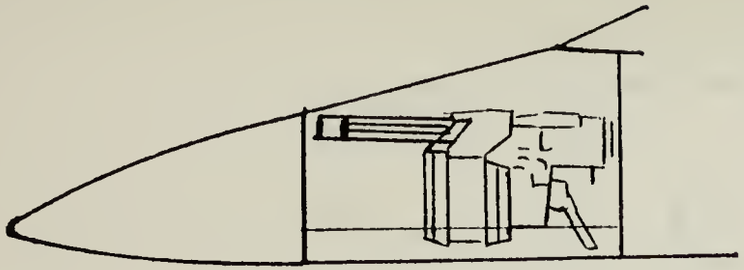

1. Basic Aircraft with Gun

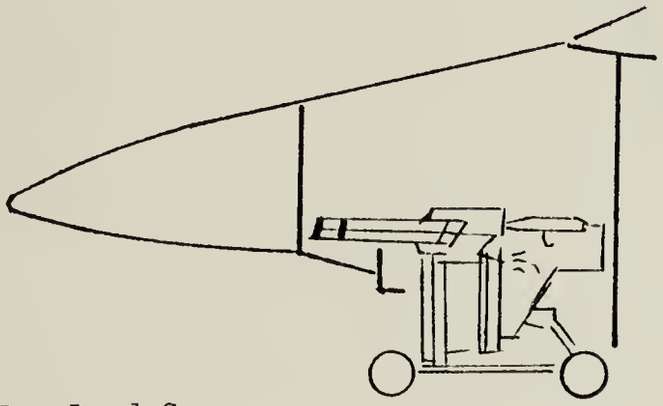

2. Download Gun

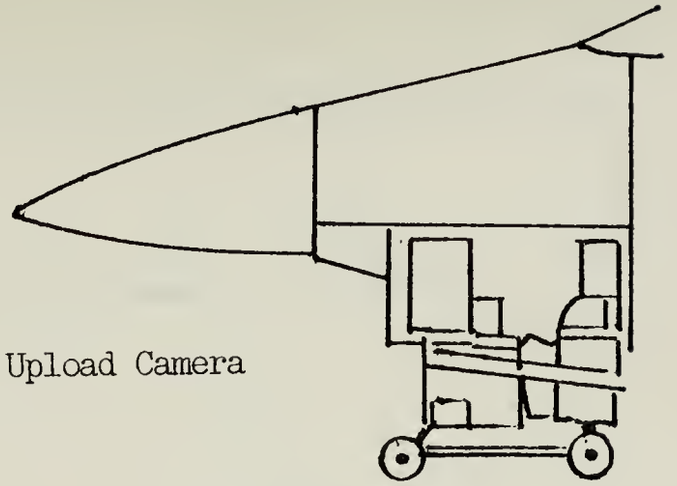

3. Upload Camera

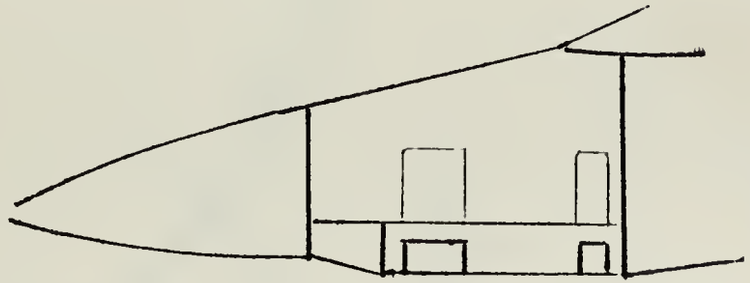

4. Reconnaissance Aircraft

FIGURE 1. Gun Removal

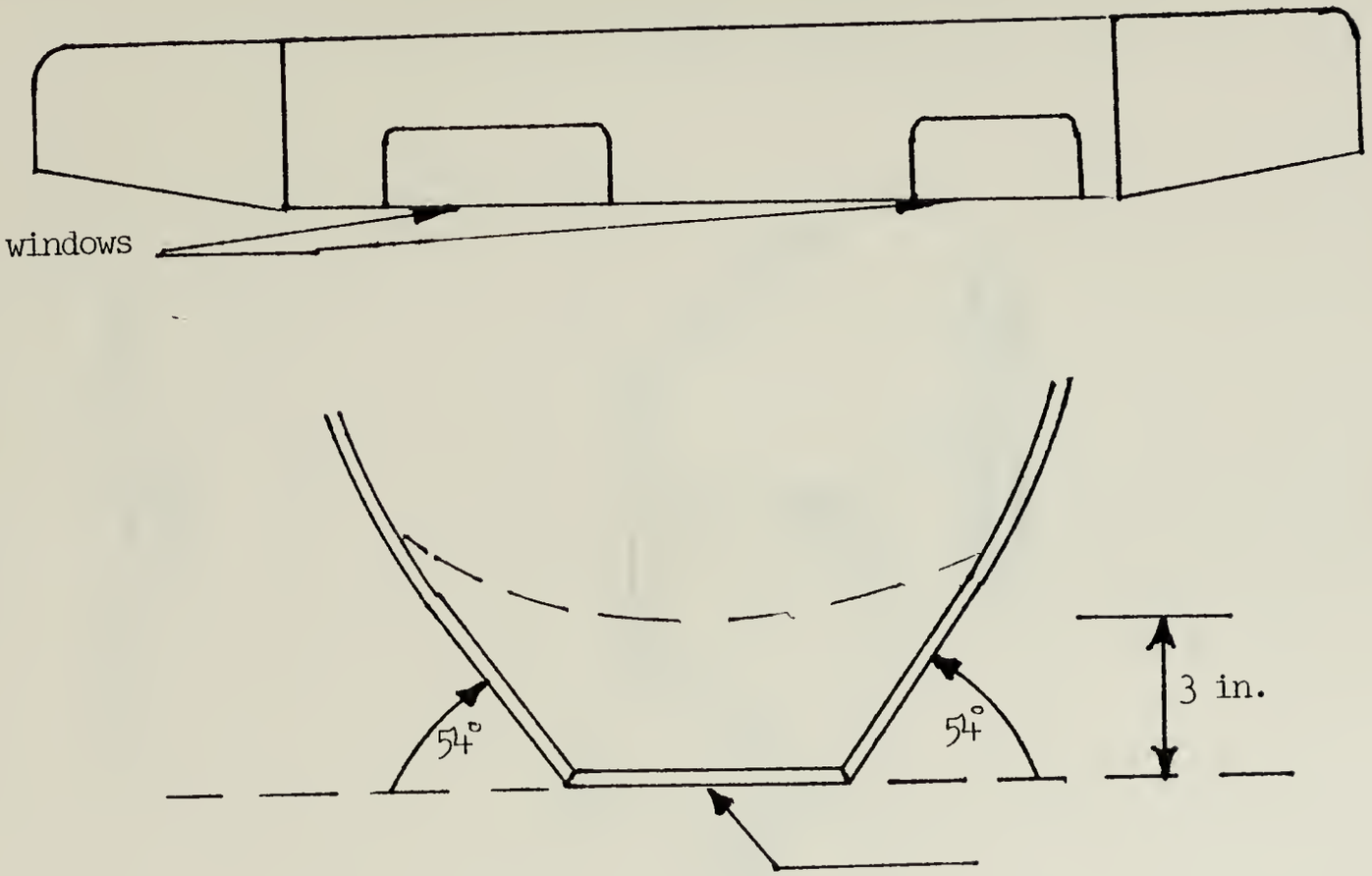

FIGURE 2. Reconnaissance Window Pallet

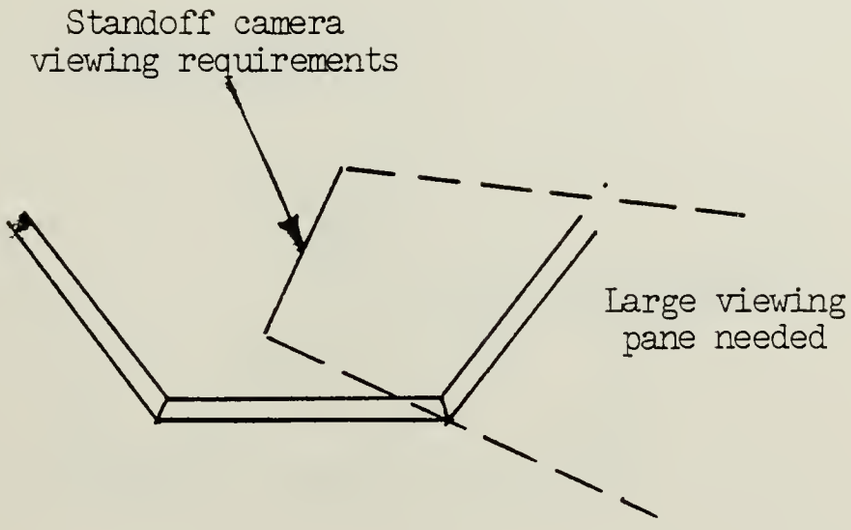

FIGURE 3.
Standoff Window Requirements

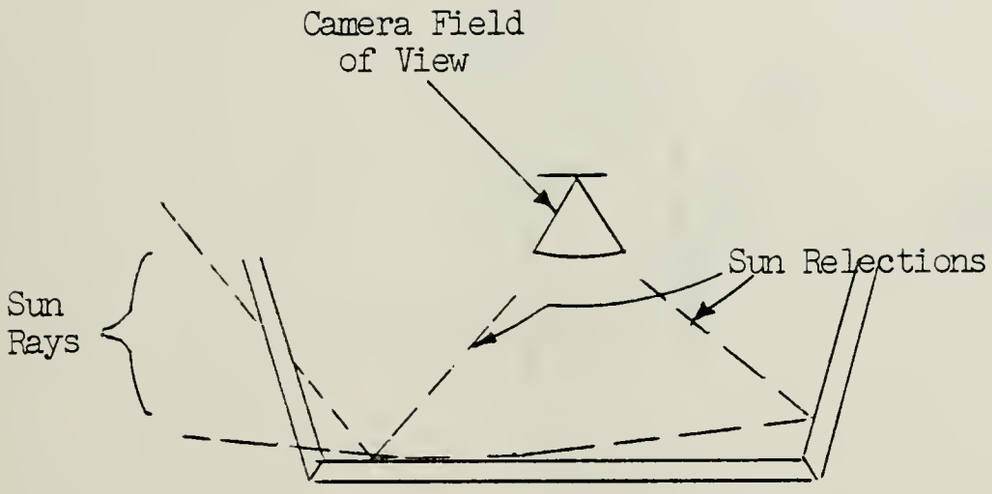

FIGURE 4.
Window Reflective Effects

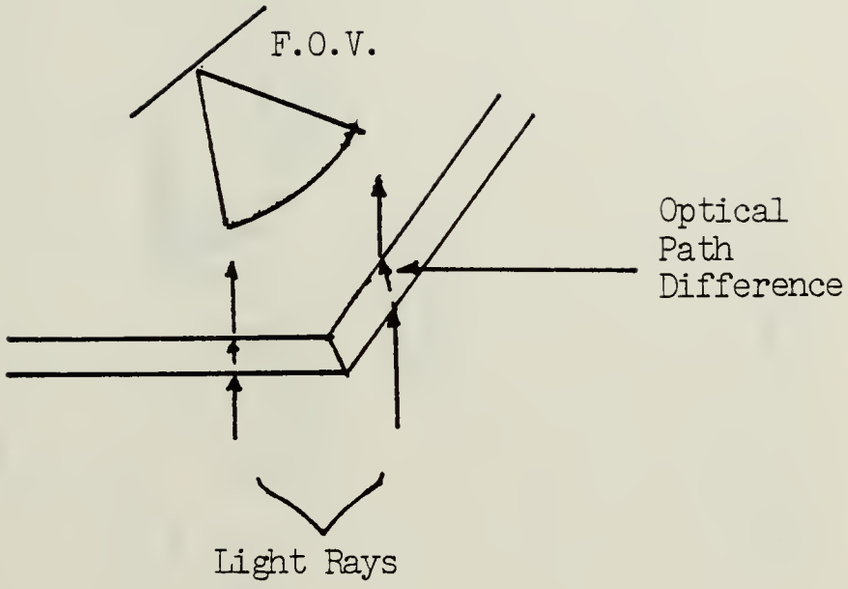

FIGURE 5
Optical Path Length Difference

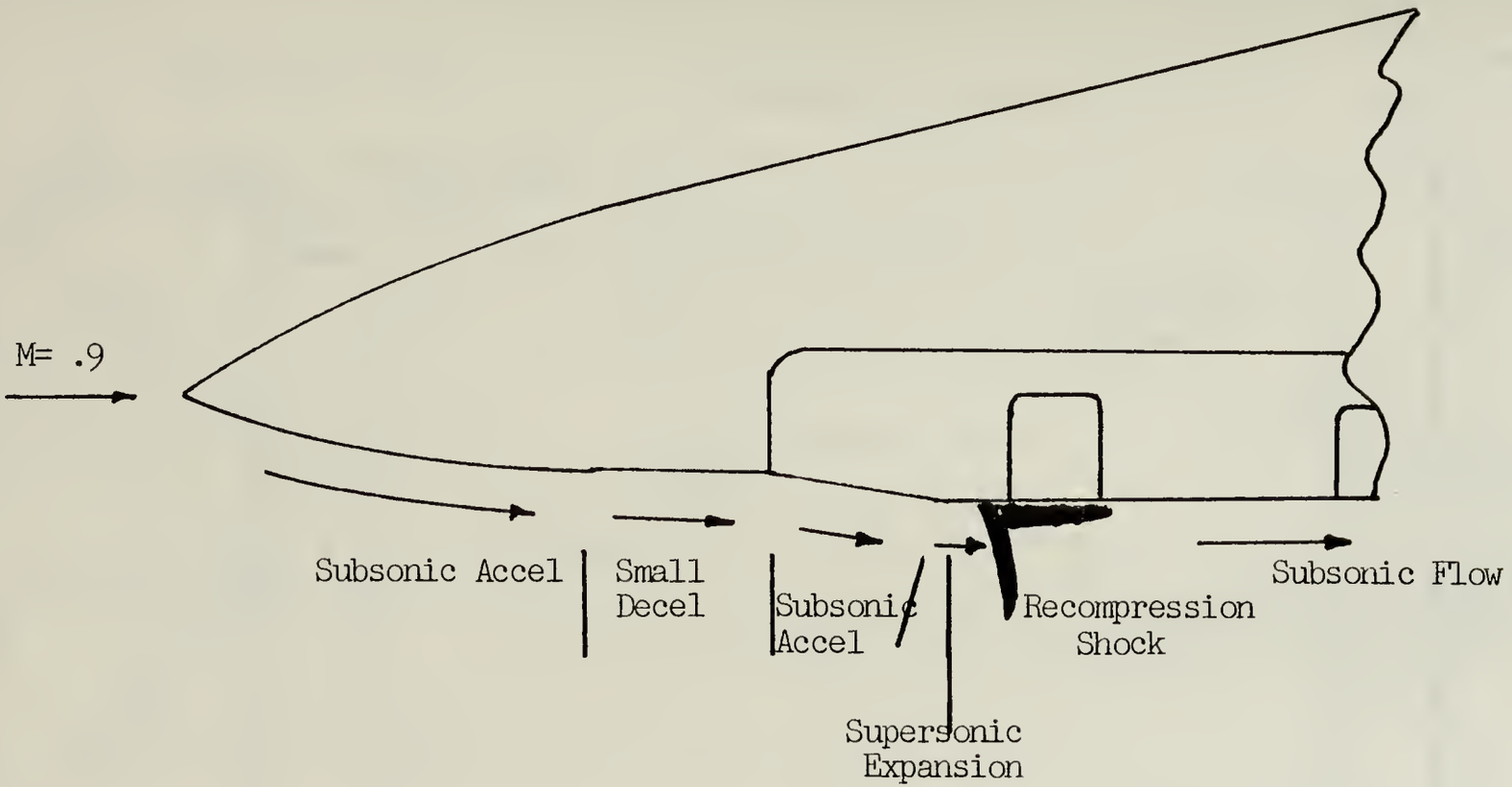

FIGURE 6. Supersonic Expansion Shock

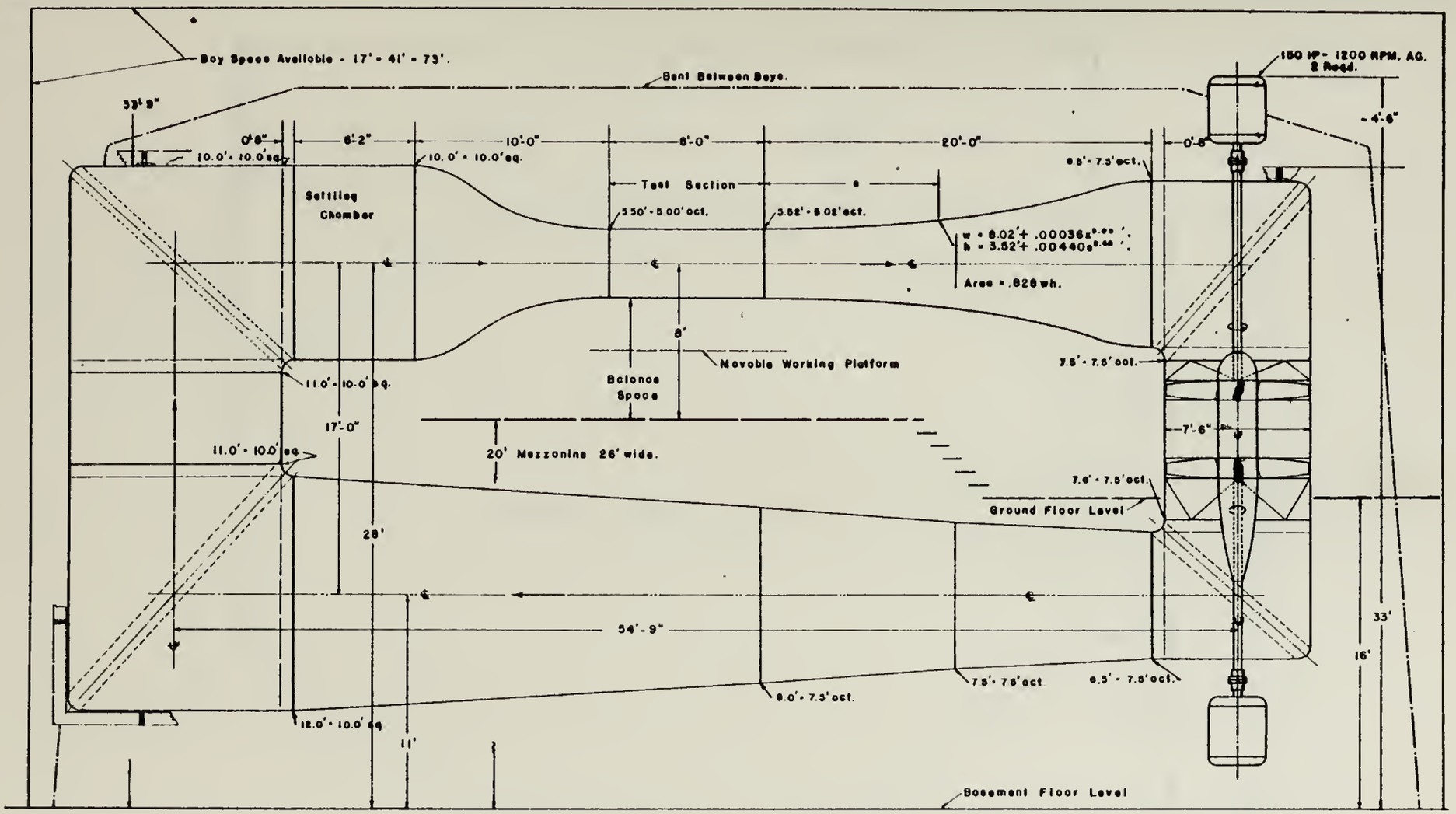

FIGURE 7.

3.5 ft. x 5.0 ft. — 200 knot ACADEMIC WIND TUNNEL.

U. S. NAVAL POSTGRADUATE SCHOOL.

Overall Dimensions: 11½' - 38' - 65½'.

MONTEREY, CALIFORNIA.

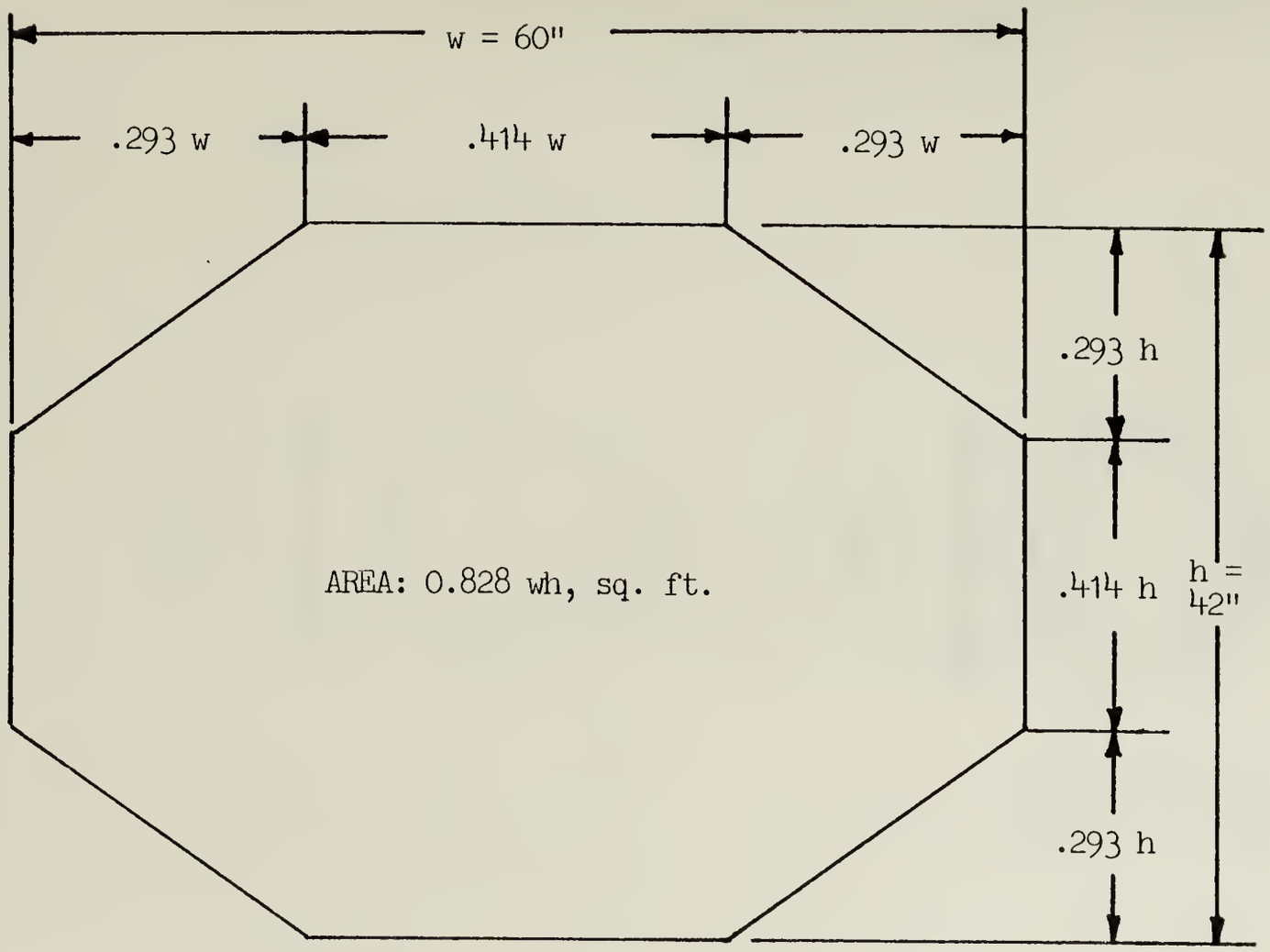

FIGURE 8. Windtunnel Test Section

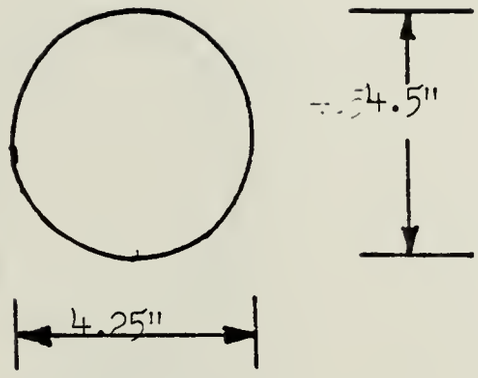

Y 128.5

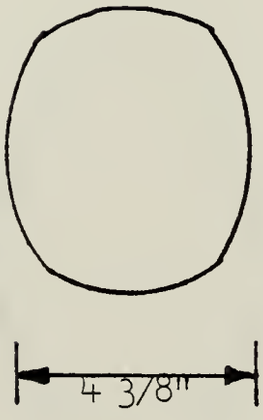

Y 152.25

FIGURE 9. Model Aircraft Dimensions

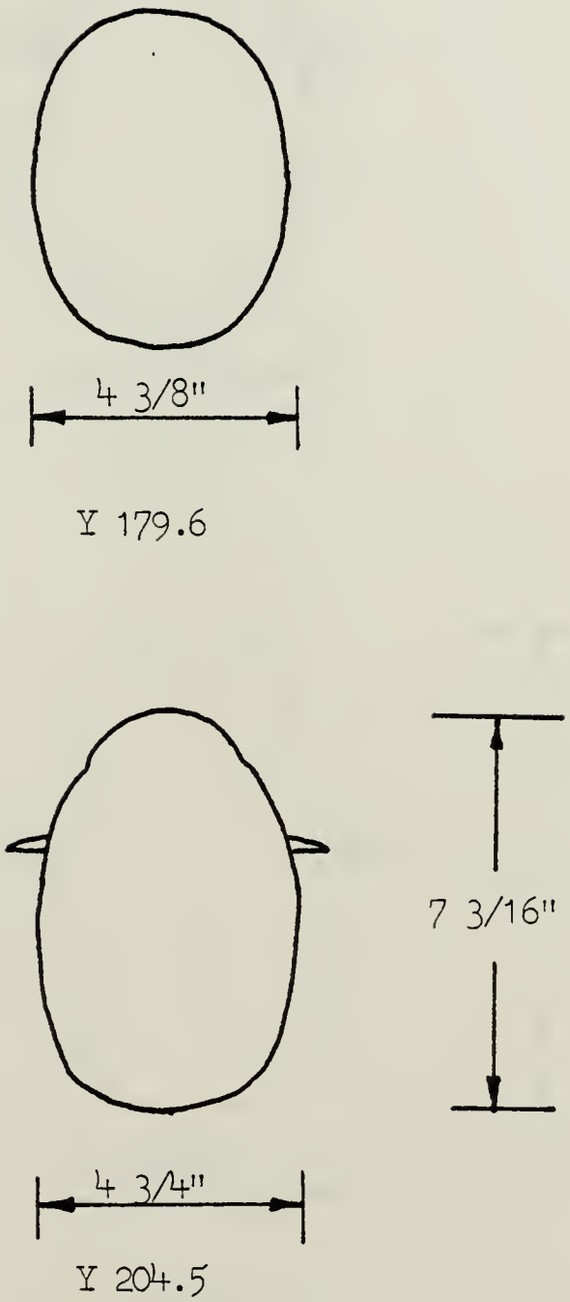

FIGURE 10. Model Aircraft Dimensions

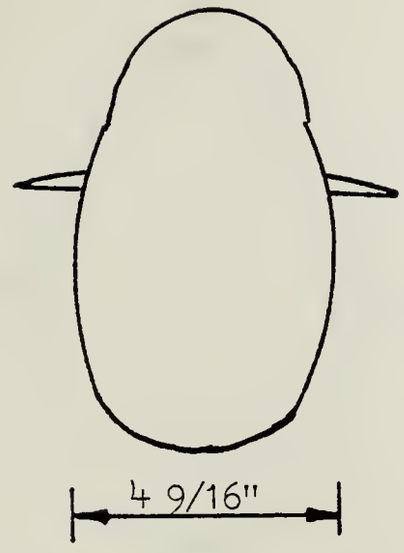

Y 218.5

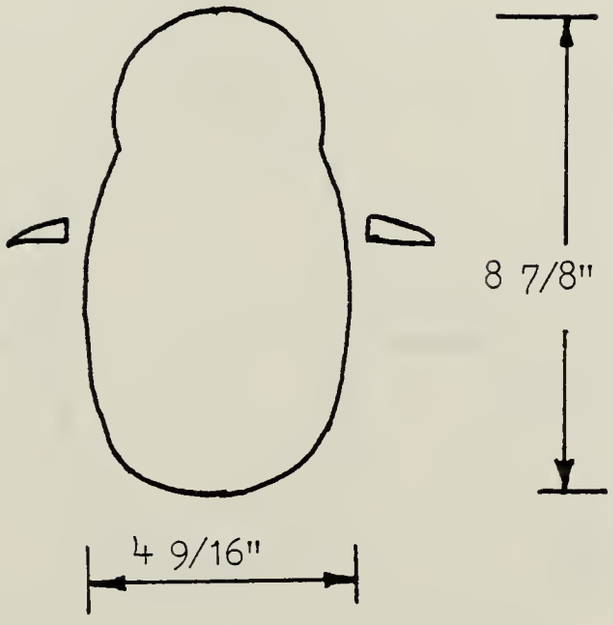

Y 233.7

FIGURE 11. Model Aircraft Dimensions

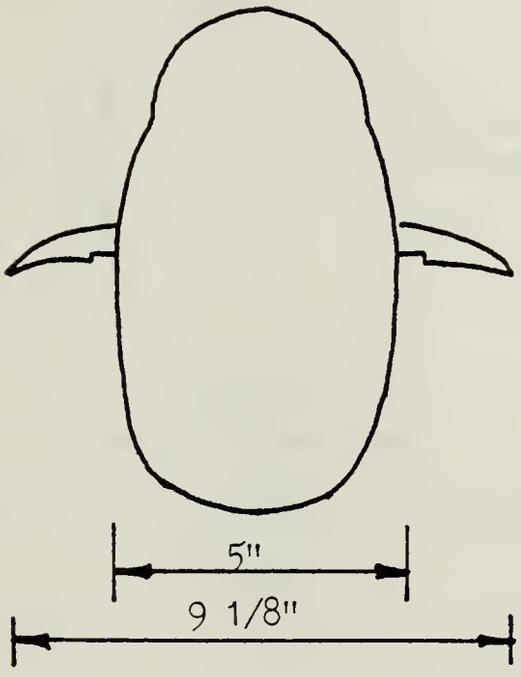

Y 279.0

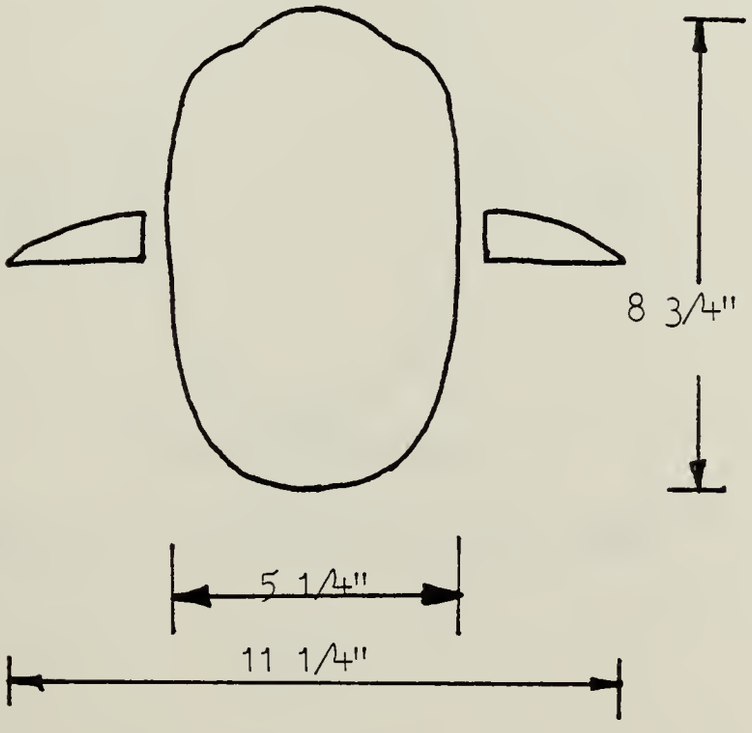

Y 311.0

FIGURE 12. Model Aircraft Dimensions

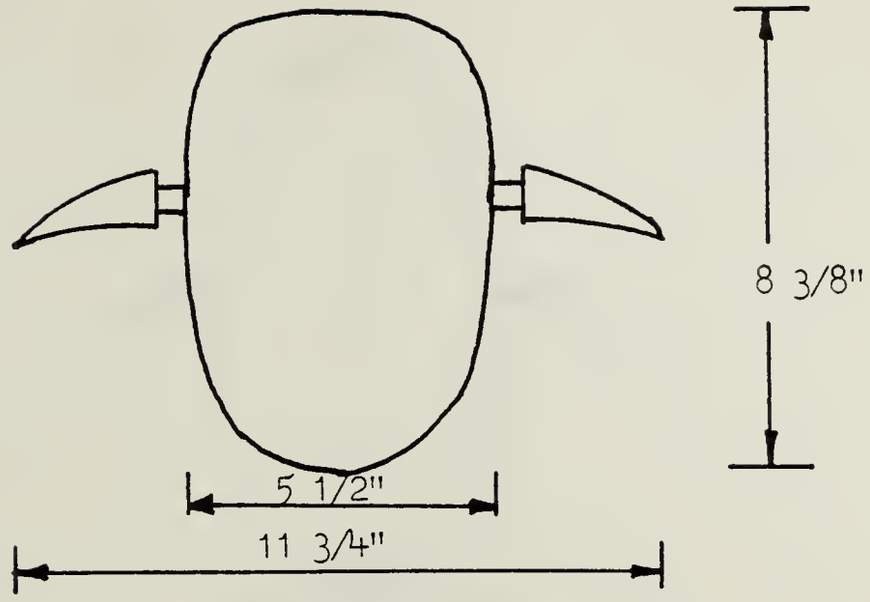

Y 326.5

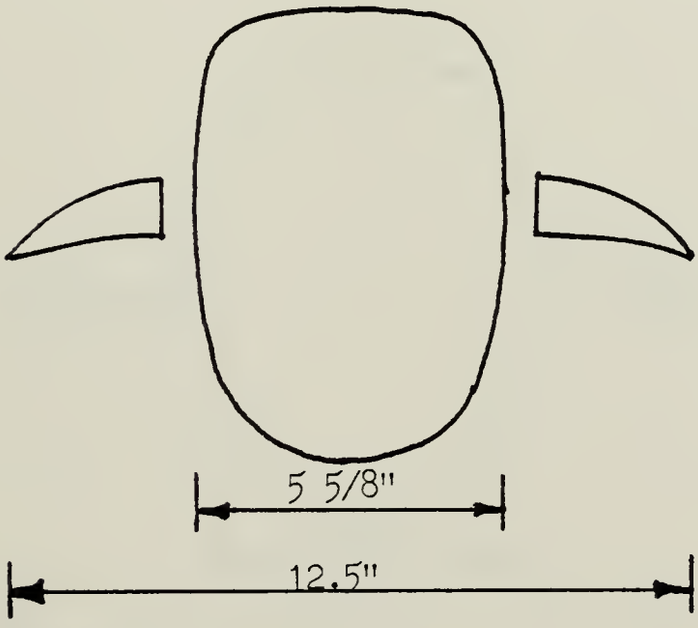

Y 347.6

FIGURE 13. Model Aircraft Dimensions

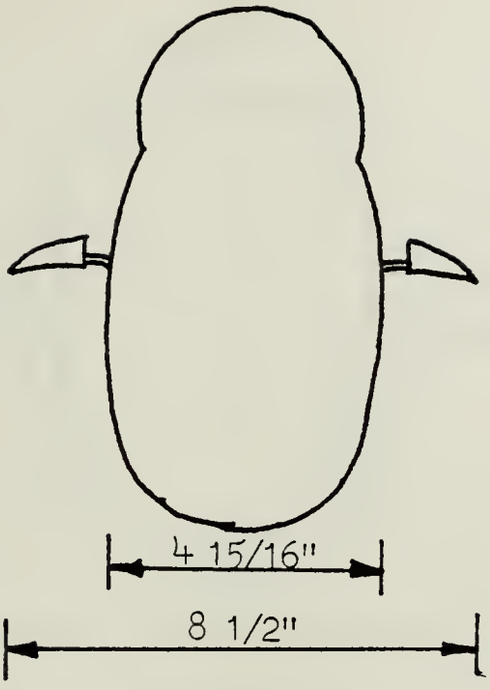

Y 260.67

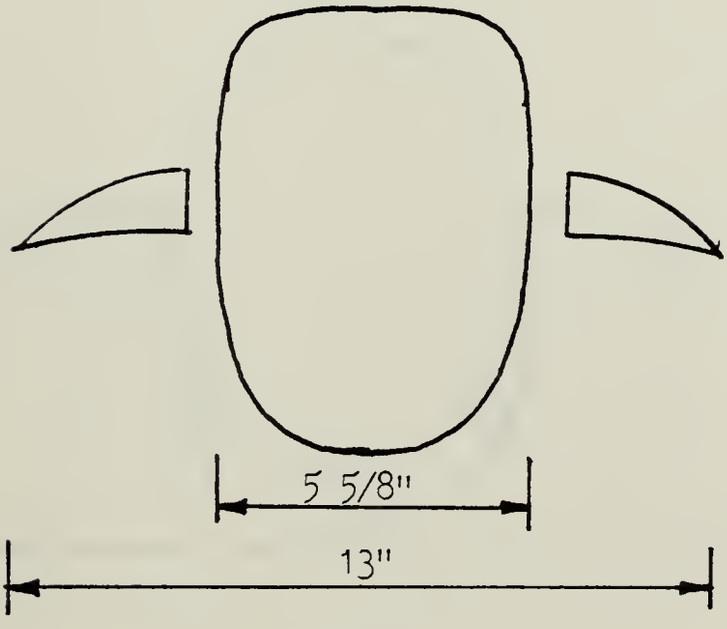

Y 357.5

FIGURE 14. Model Aircraft Dimensions

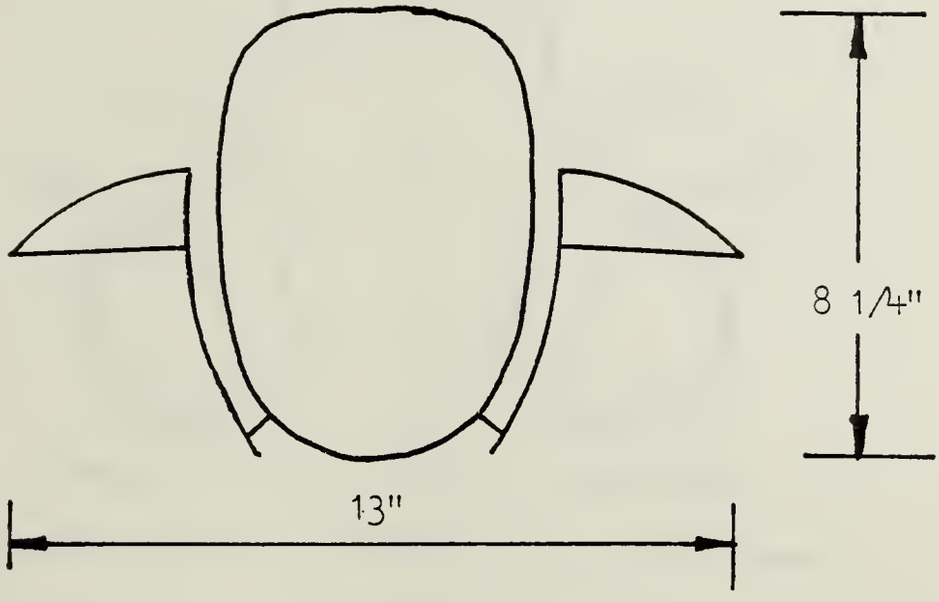

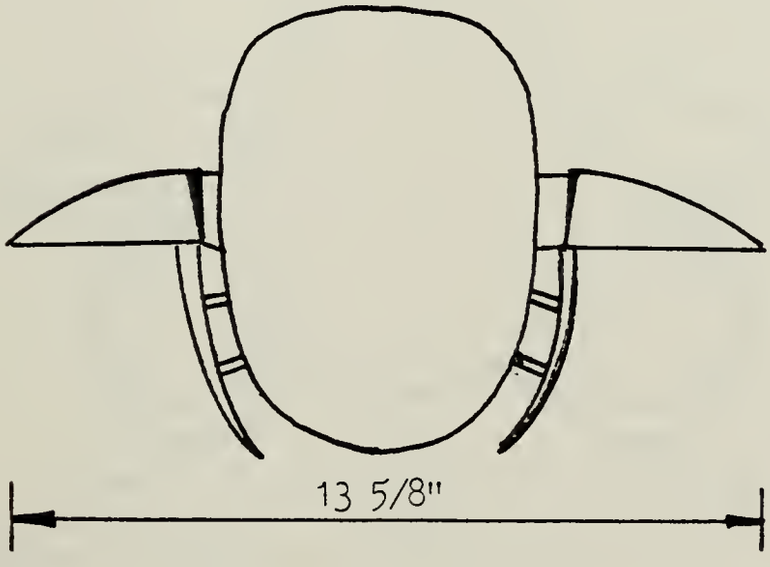

FIGURE 15. Model Aircraft Dimensions

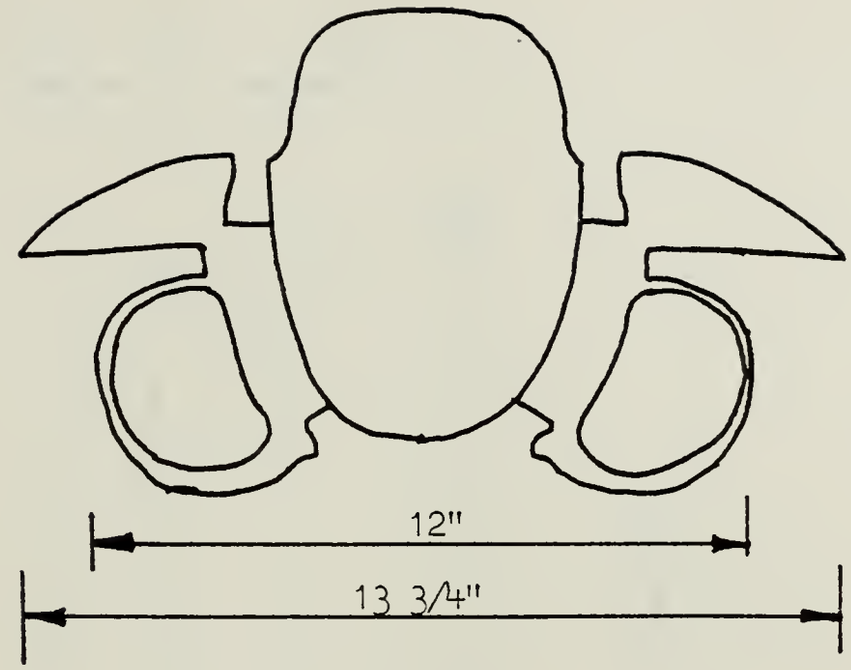

Y 419.0

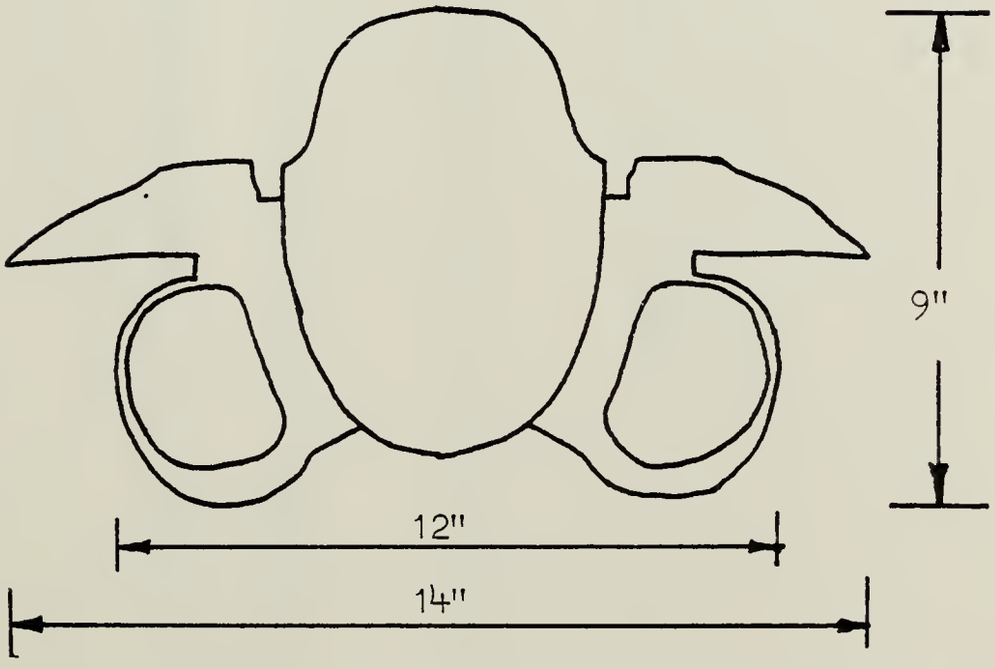

Y 427.0

FIGURE 16. Model Aircraft Dimensions

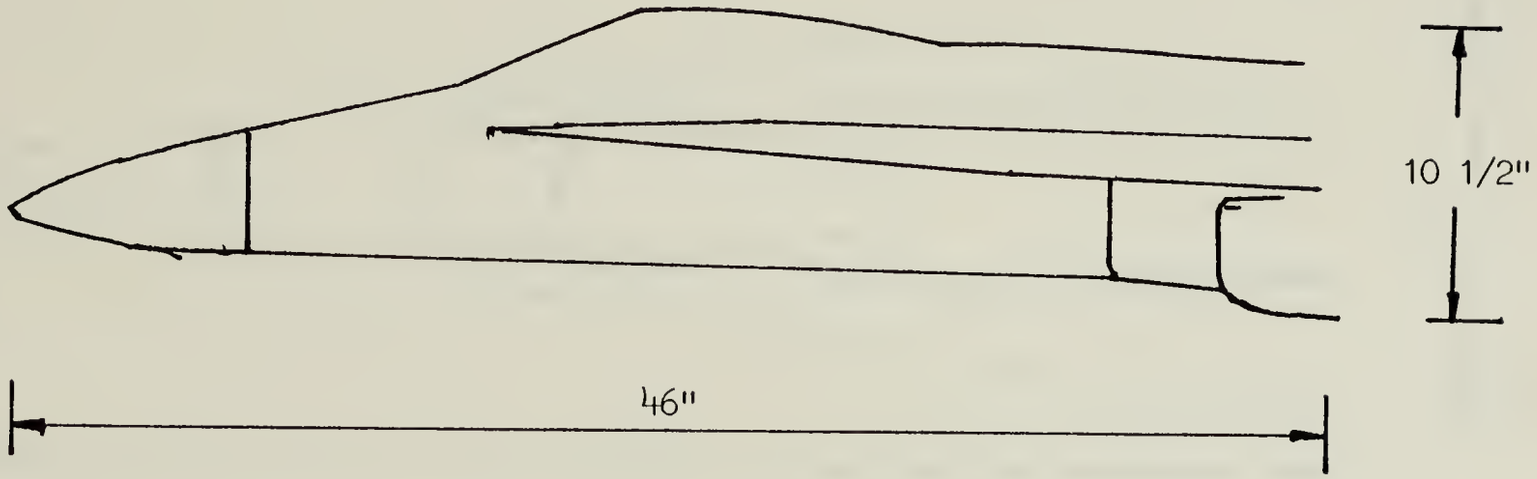

FIGURE 17. Model Aircraft Dimensions

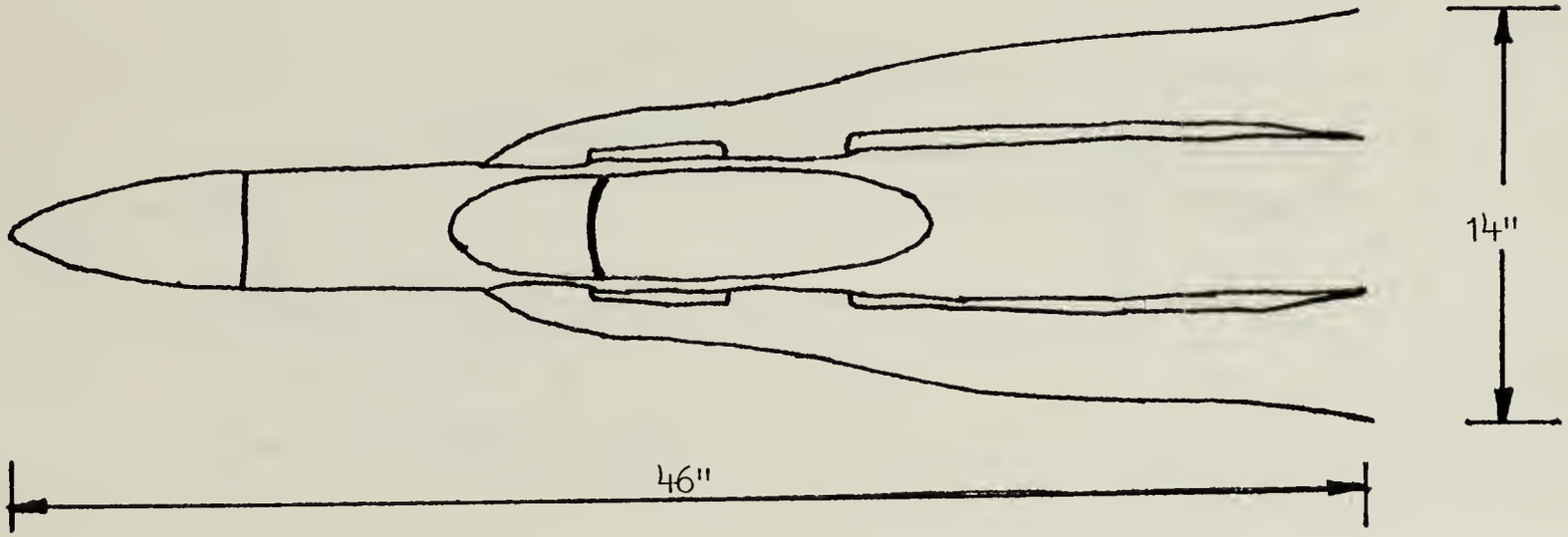

FIGURE 18. Model Aircraft Dimensions

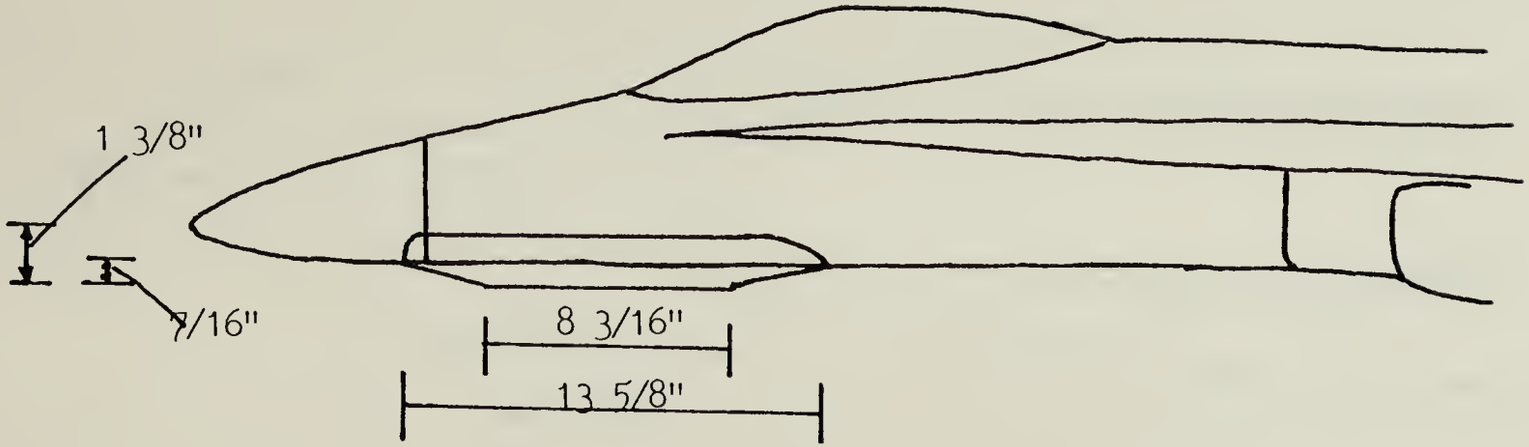

FIGURE 19. Model Aircraft Dimensions

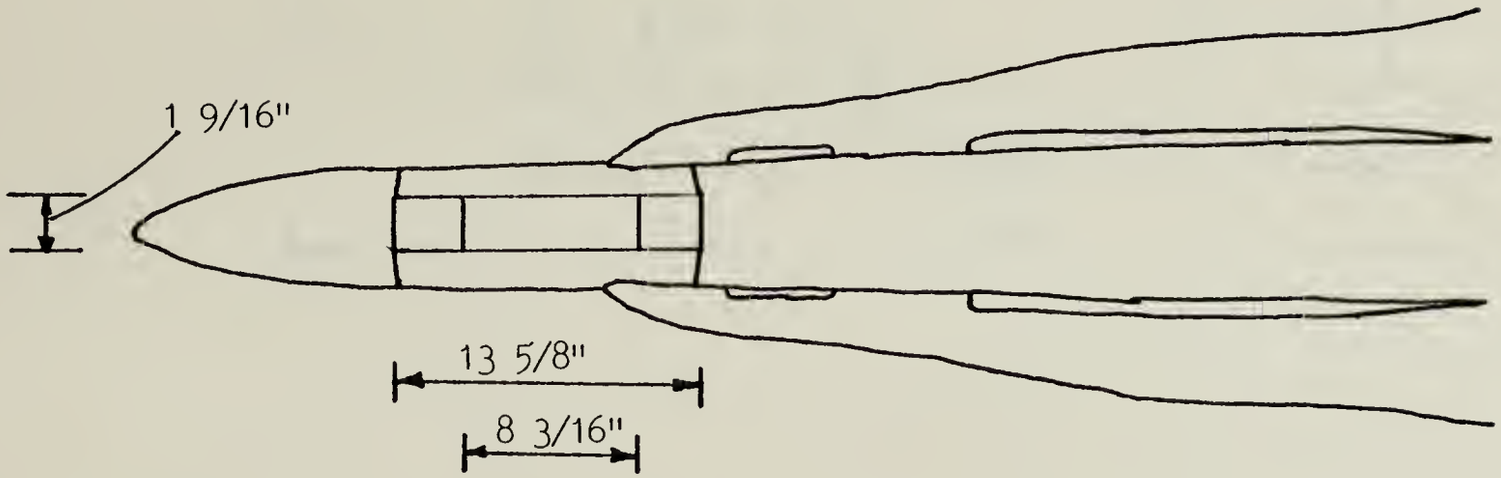

FIGURE 20. Model Aircraft Dimensions

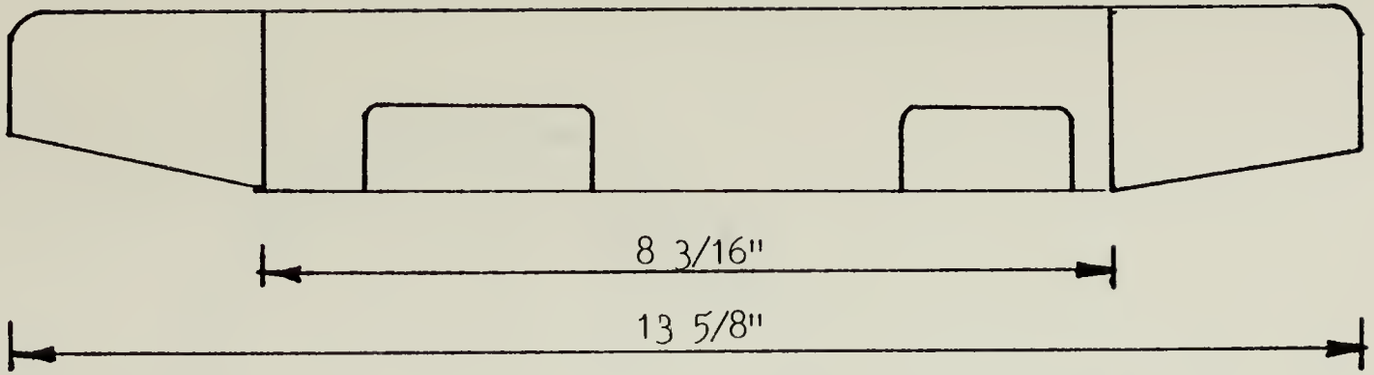

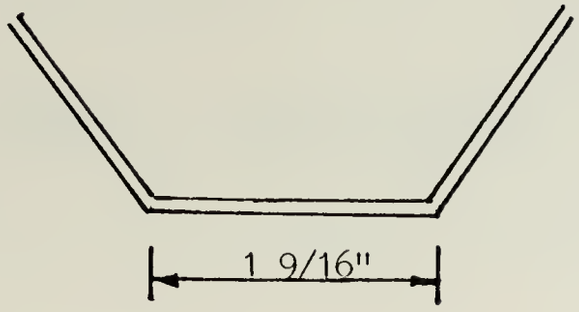

FIGURE 21. Model Window Pallet Dimensions

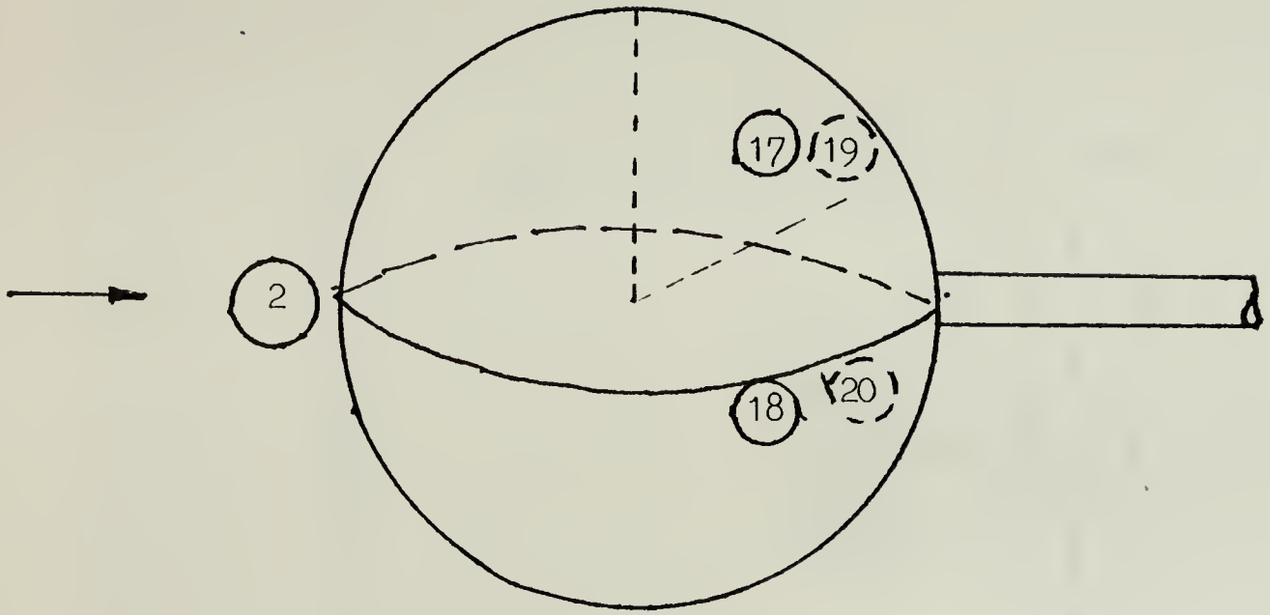

FIGURE 22. Turbulence Sphere

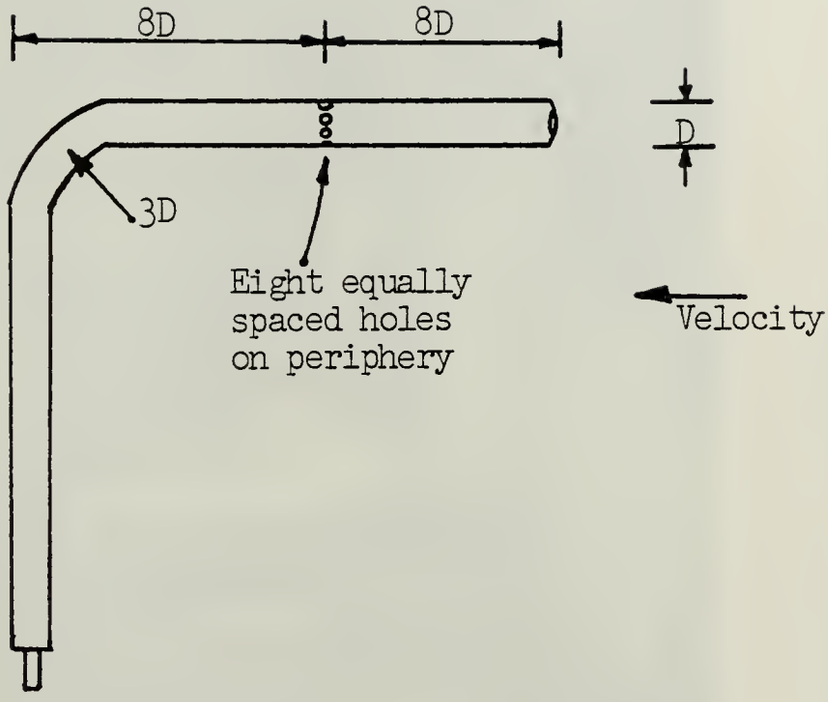

FIGURE 23. Pitot Static Probe

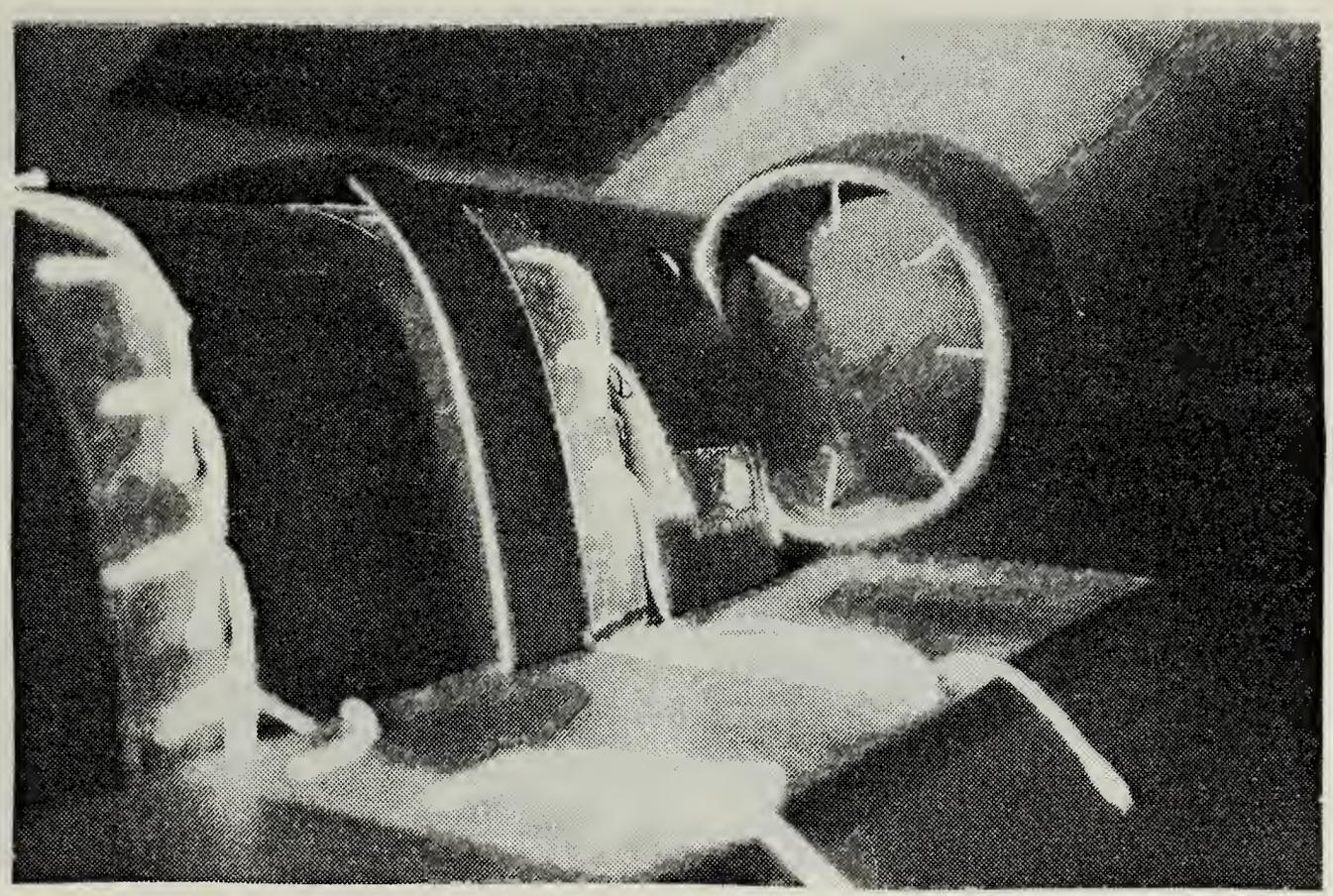

FIGURE 24. Intake Pressure Probes

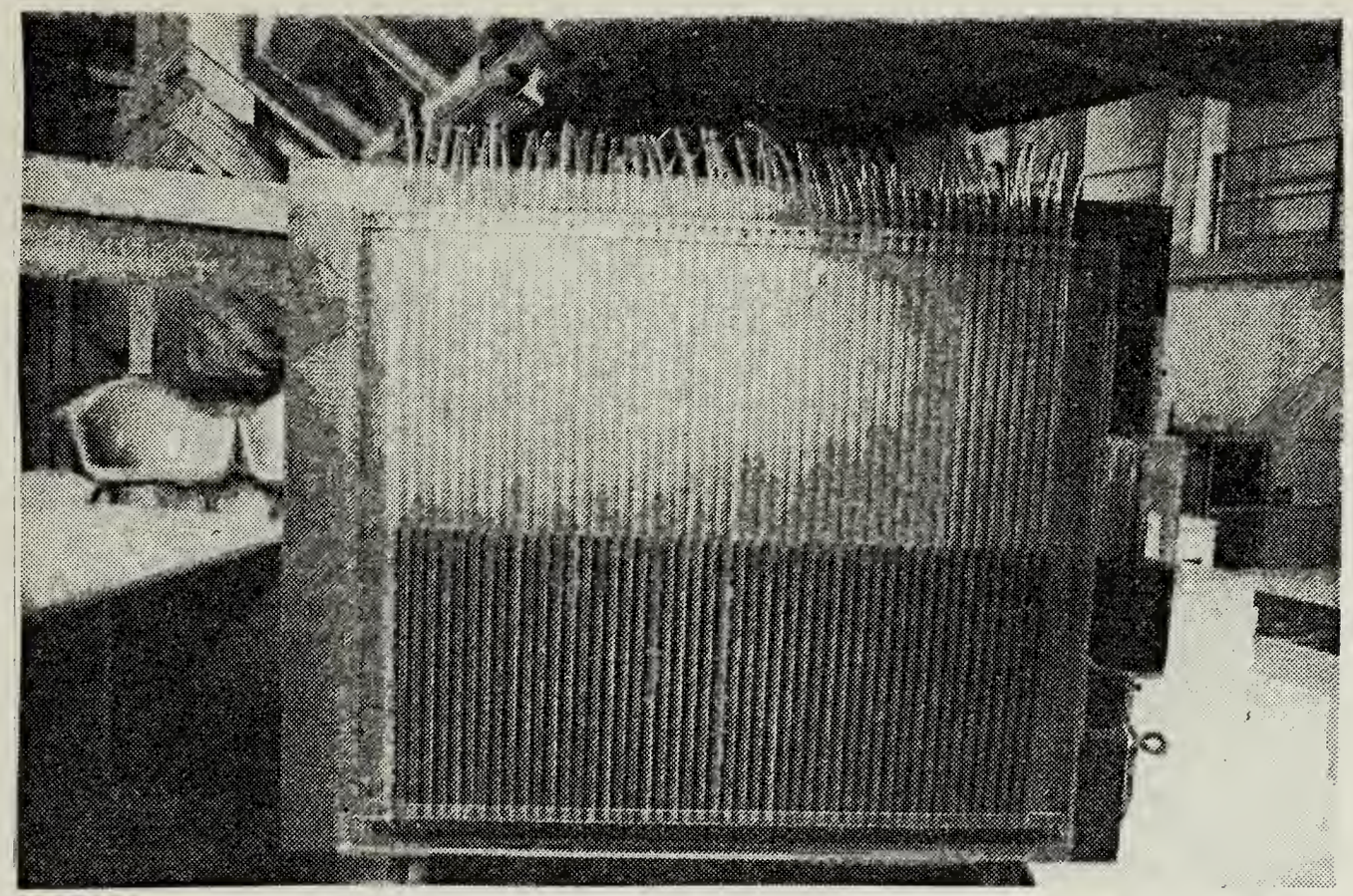

FIGURE 25. Manometer Board

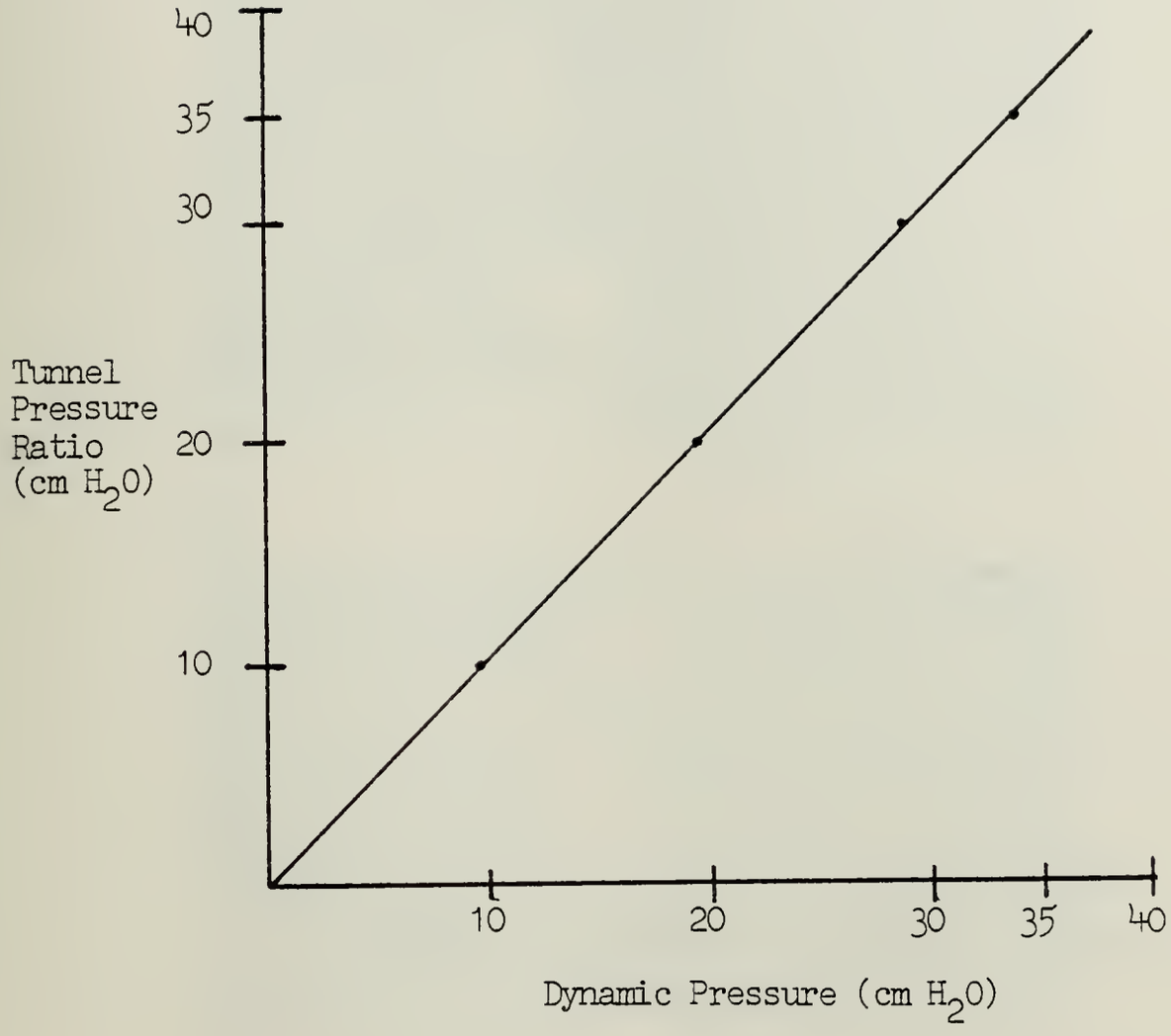

FIGURE 26. Tunnel Calibration Factor

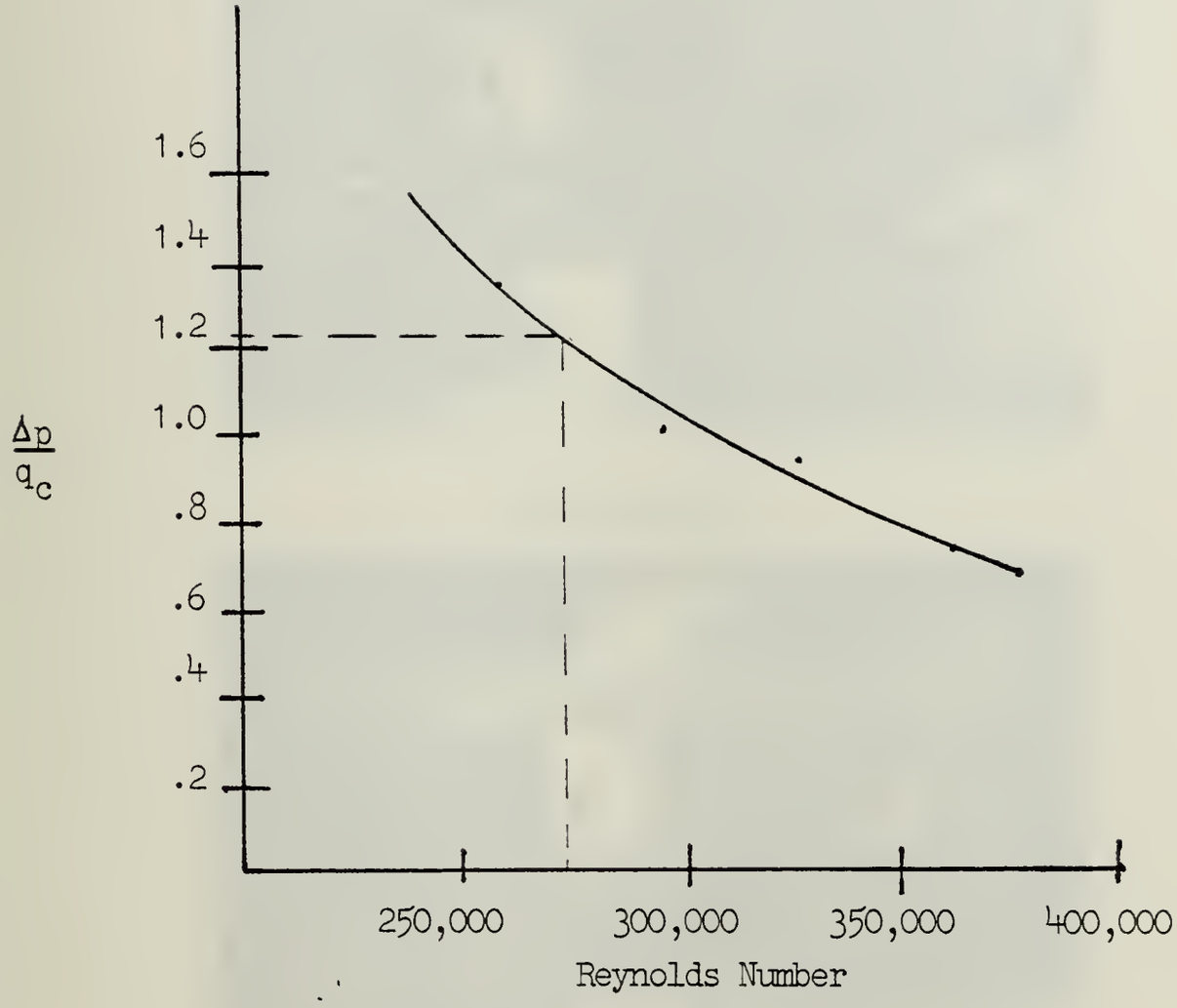

FIGURE 27. Tunnel Turbulence Factor

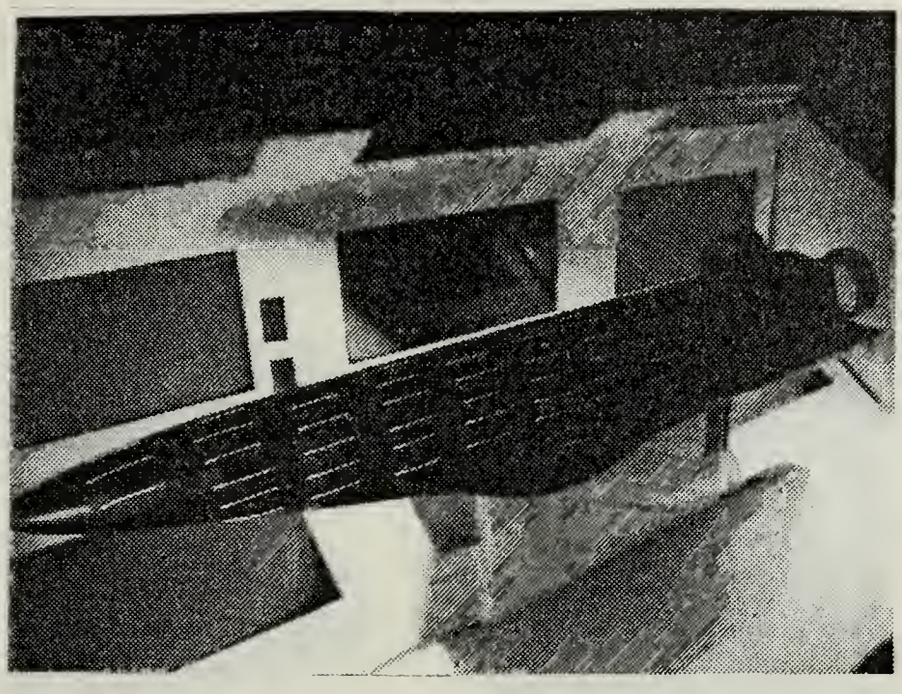

Base Aircraft

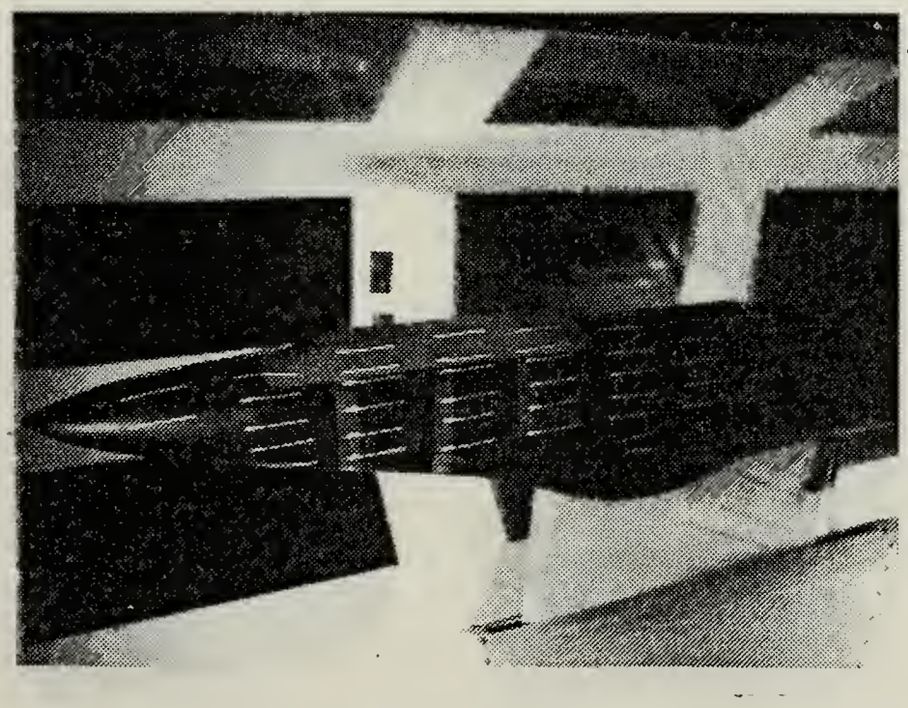

Modified Aircraft

FIGURE 28. 0^{o} Angle of Attack Comparison

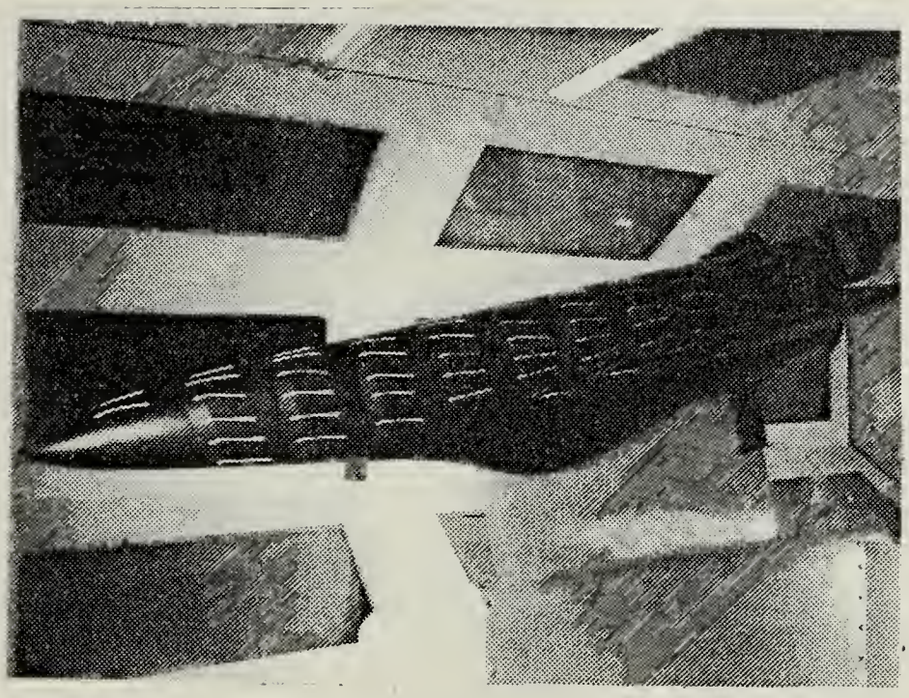

Base Aircraft

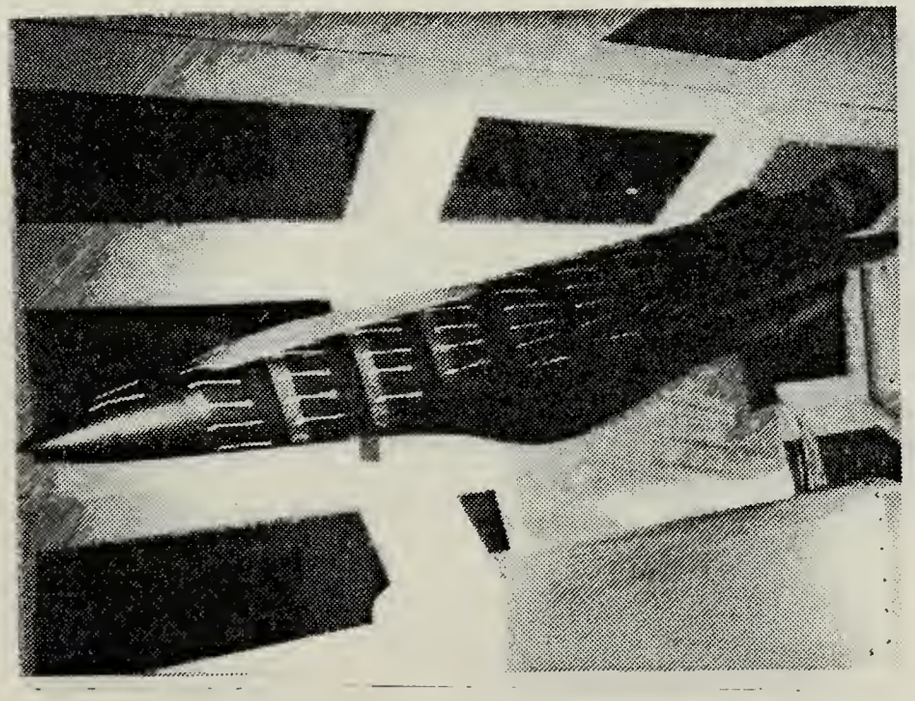

Modified Aircraft

FIGURE 29. +12° Angle of Attack Comparison

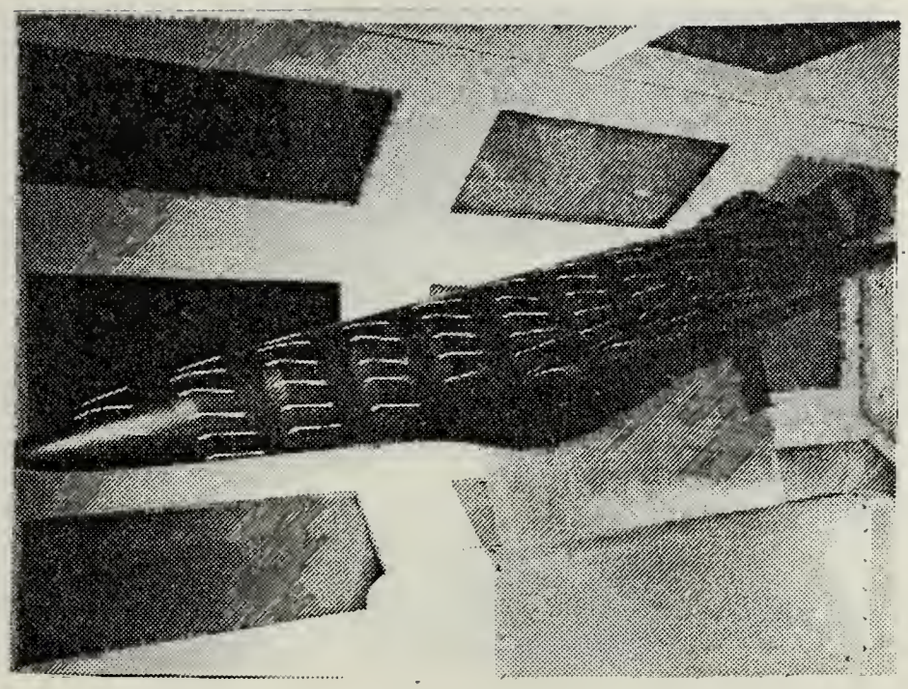

Base Aircraft

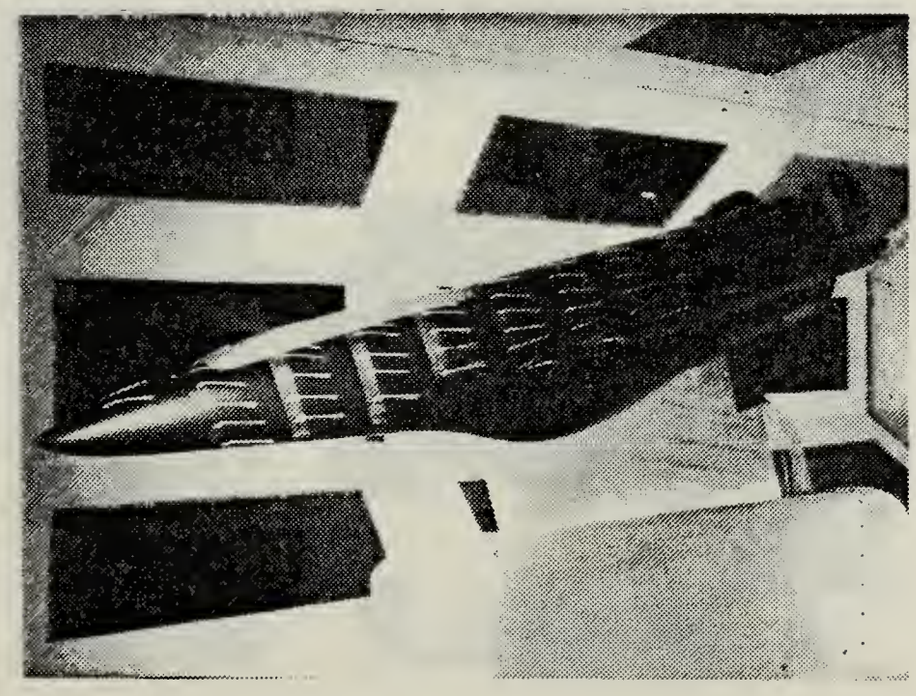

Modified Aircraft

FIGURE 30. $+15^{o}$ Angle of Attack Comparisons

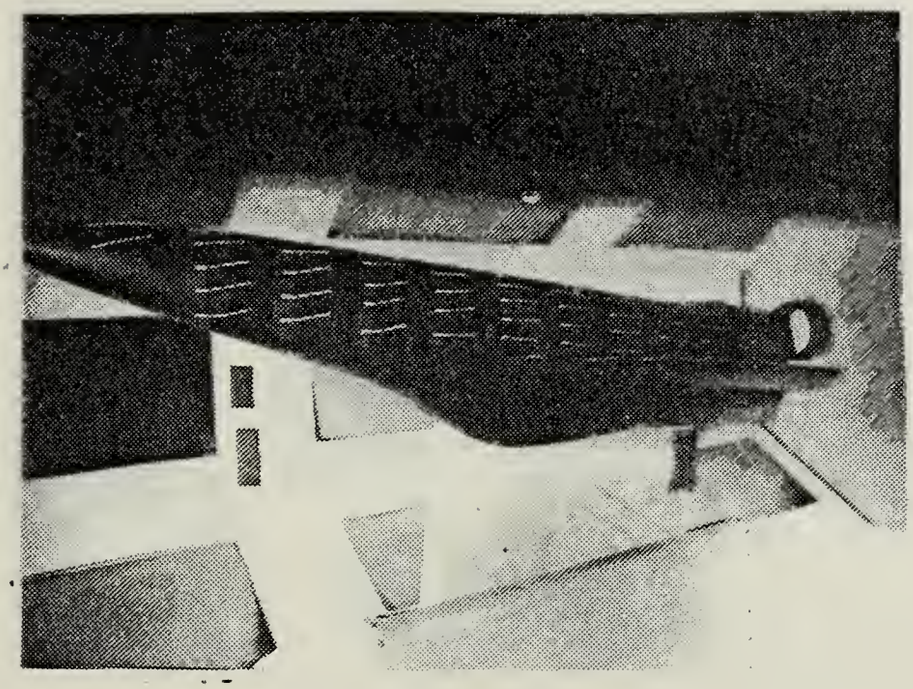

Base Aircraft

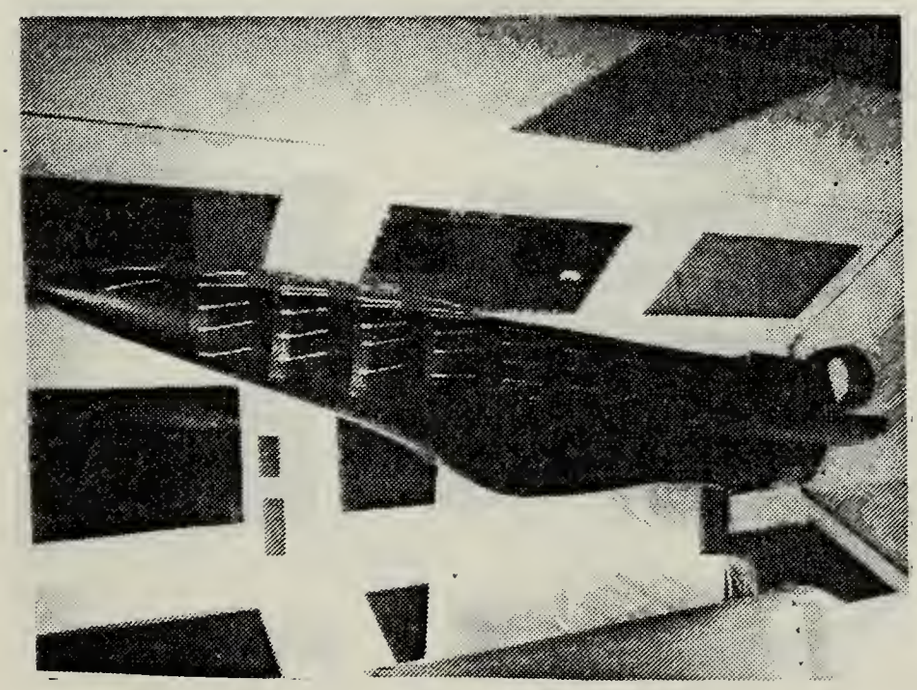

Modified Aircraft

FIGURE 31. -8° Angle of Attack Comparison

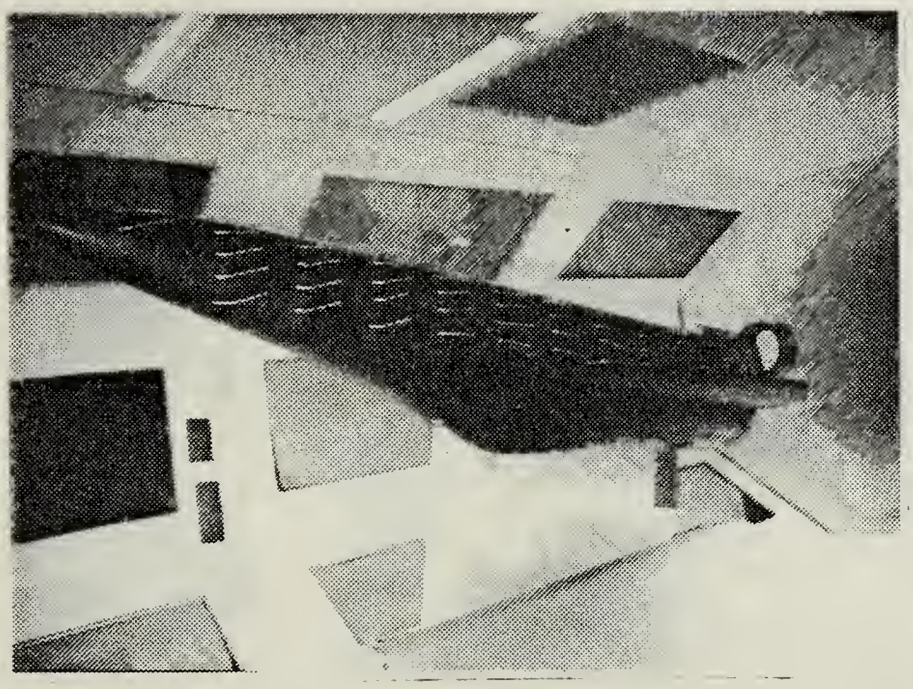

Base Aircraft

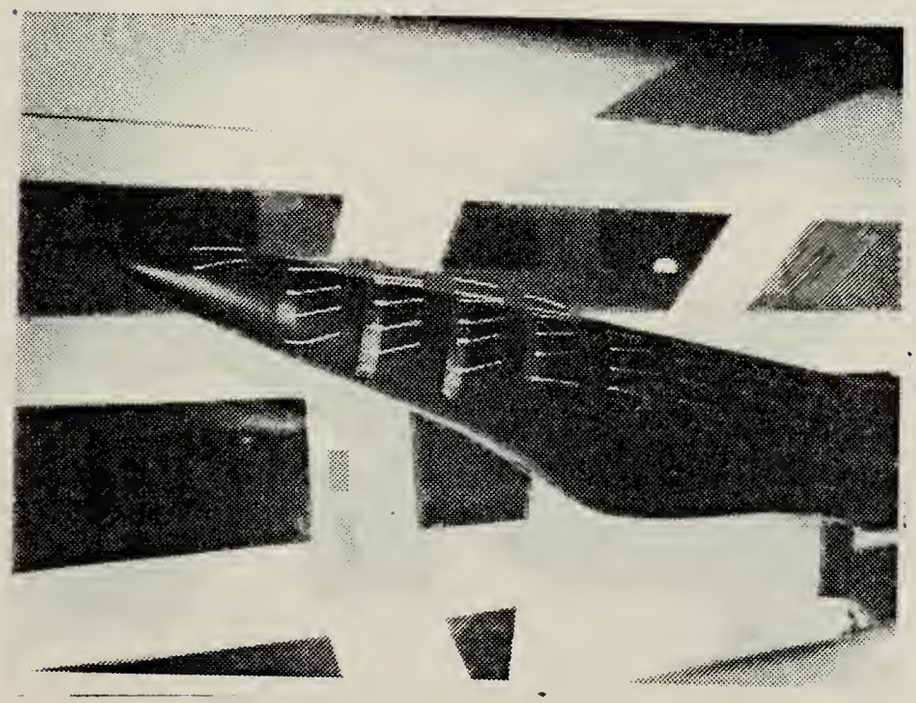

Modified Aircraft

FIGURE 32. -15° Angle of Attack Comparison

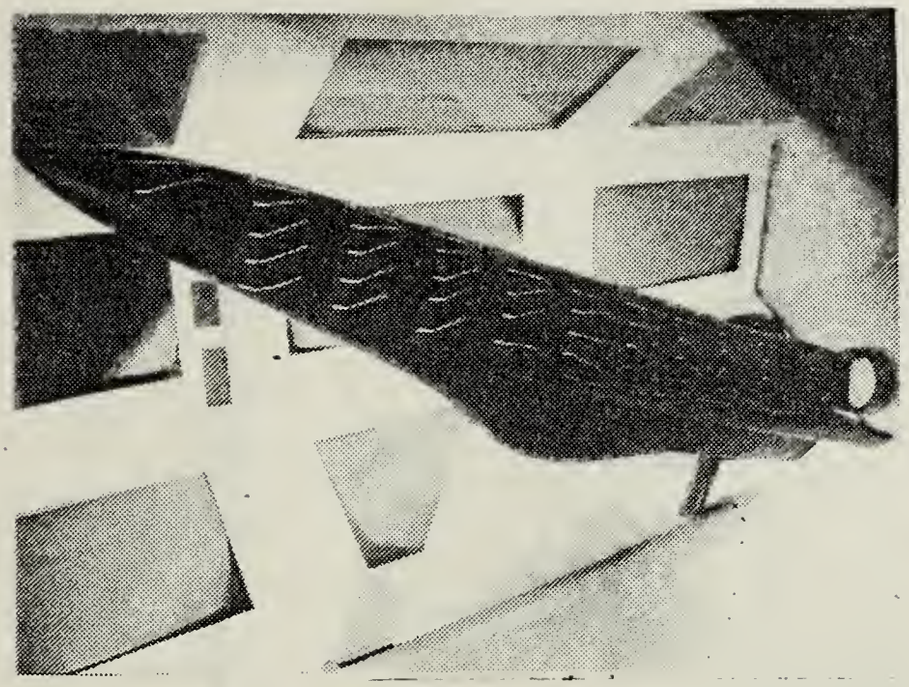

Base Aircraft

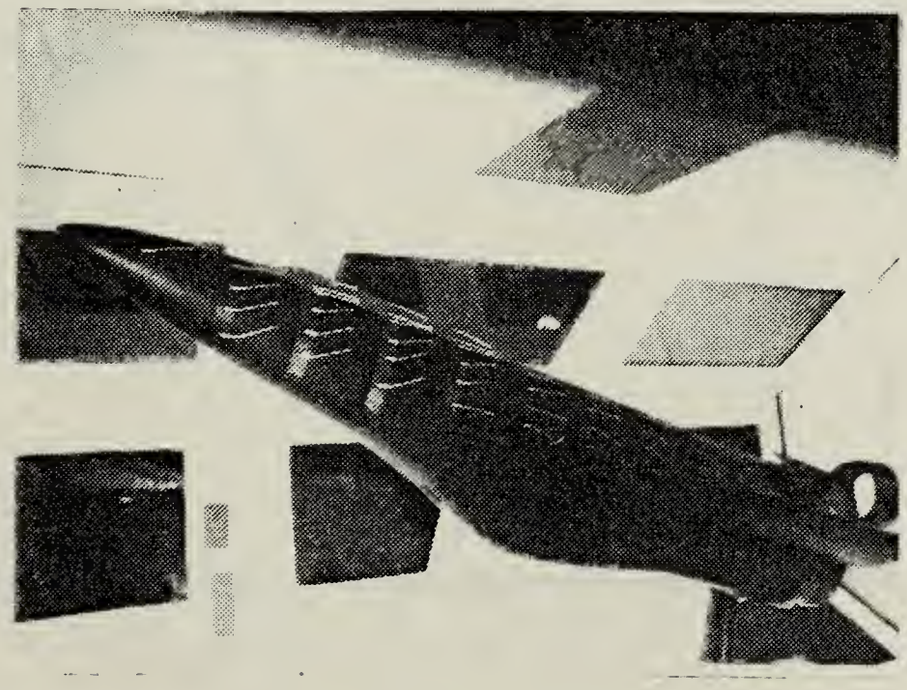

Modified Aircraft

FIGURE 33. -20° Angle of Attack Comparison

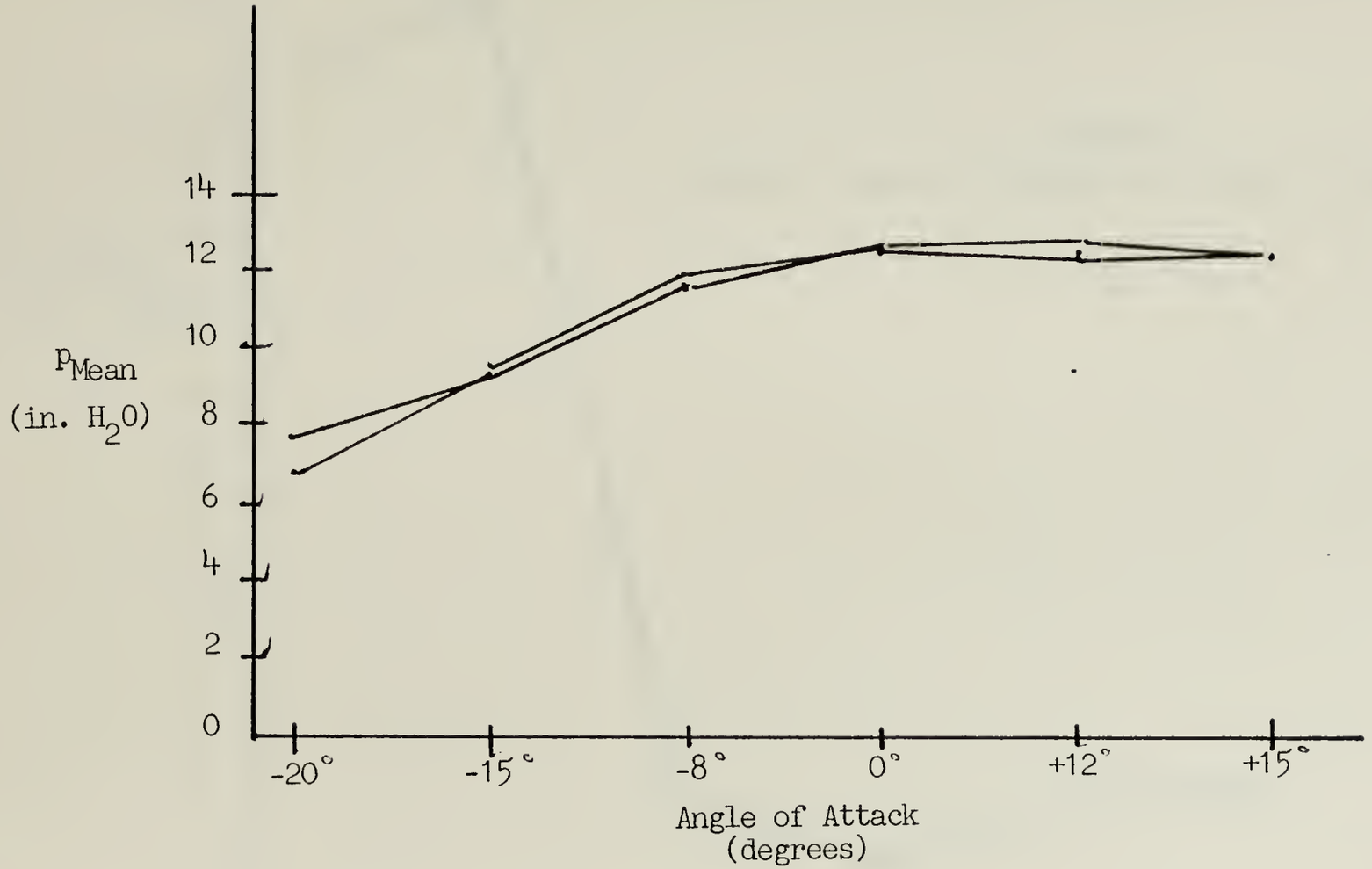

FIGURE 34. Pressure Mean vs. Angle of Attack

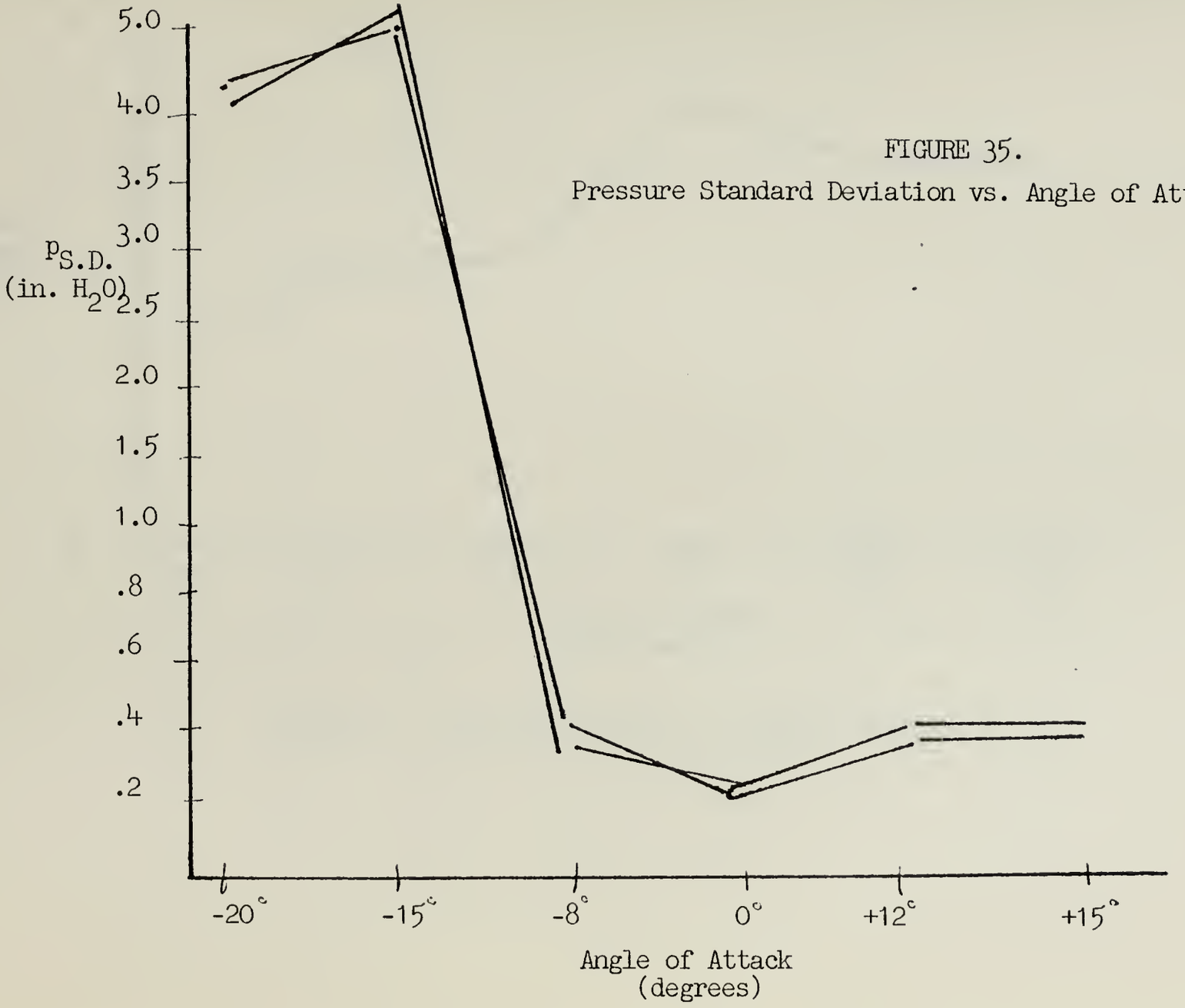

FIGURE 35.

Pressure Standard Deviation vs. Angle of Attack

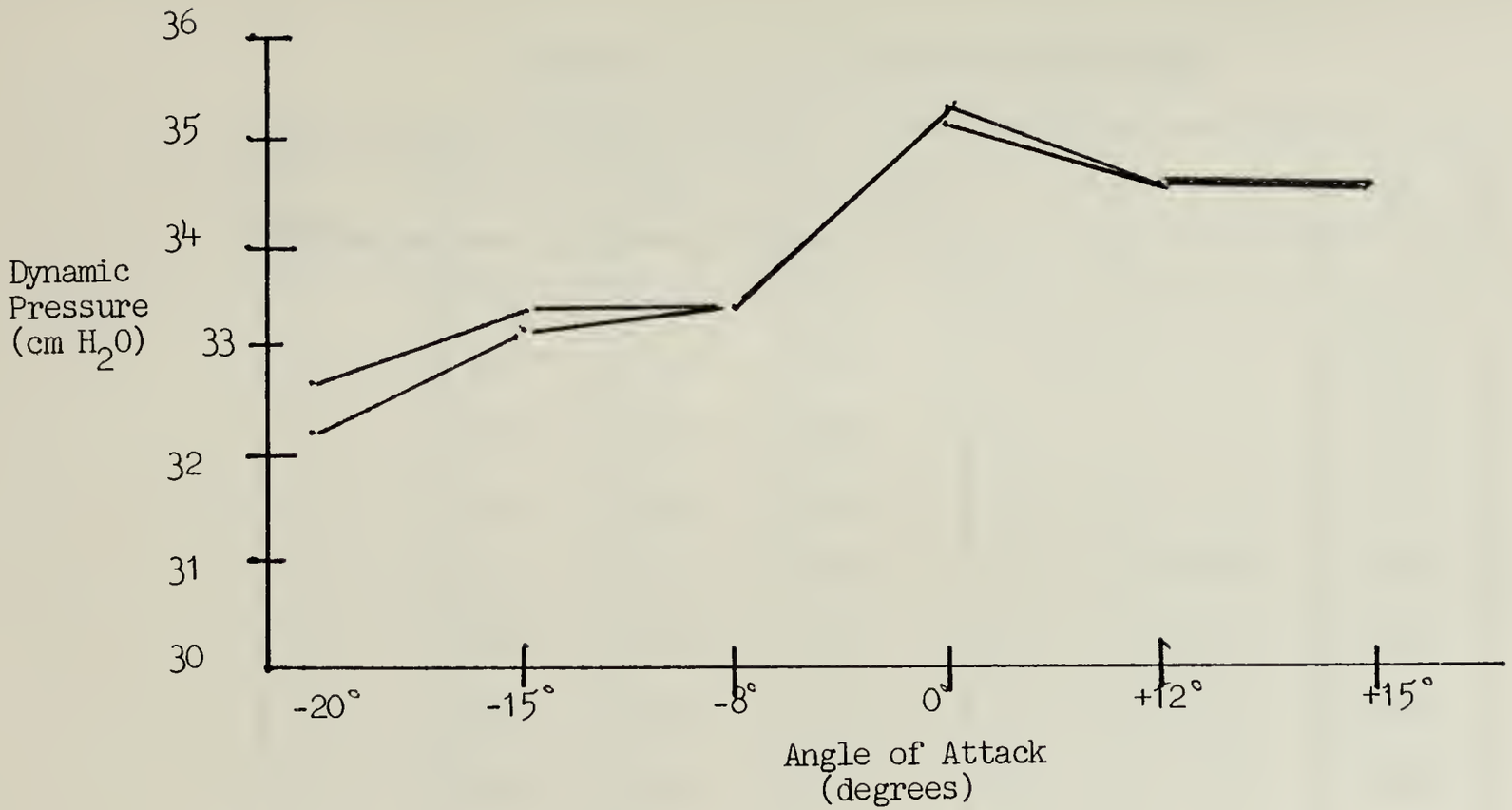

FIGURE 36. Dynamic Pressure vs. Angle of Attack

FIGURE 37. Base Aircraft Pressures (Δp)

probe	0	+12	+15	-8	-15	-20
1.	12.5	12.2	12.6	12.2	12.1	10.3
2.	12.0	11.1	11.4	11.95	12.0	9.4
3.	12.5	12.2	12.6	12.2	10.0	1.2
4.	12.5	12.3	12.7	12.2	-4.3	-1.1
5.	12.5	12.32	12.75	12.2	10.8	9.15
6.	12.5	12.35	12.8	12.2	12.2	9.9
7.	12.5	12.2	12.45	12.0	12.0	10.0
8.	12.5	12.0	12.1	12.0	12.05	10.05
9.	12.0	12.1	12.1	11.8	9.5	2.2
10.	12.6	12.7	12.85	12.1	.5	2.9
11.	11.9	11.95	11.95	10.8	10.1	8.9
12.	12.6	12.9	12.9	12.2	12.2	9.85
Q.	35.25	34.50	34.50	33.50	33.45	32.60

FIGURE 38. Modified Aircraft Pressures

probe #	0	+12	+15	-8	-15	-20
1.	13.0	12.7	12.6	11.9	12.0	10.9
2.	12.5	12.7	12.6	11.9	11.9	10.7
3.	12.9	12.7	12.6	11.9	9.8	4.2
4.	12.9	12.8	12.7	11.9	-4.5	-1.8
5.	12.9	12.8	12.7	11.8	10.8	9.8
6.	12.8	12.8	12.75	11.9	12.0	11.1
7.	12.75	12.5	12.45	11.8	11.8	10.8
8.	12.7	12.4	12.2	11.8	12.0	11.0
9.	12.4	12.3	12.2	11.3	9.8	5.2
10.	13.0	12.7	12.5	11.9	1.4	0.3
11.	12.3	12.0	11.9	10.4	10.0	9.0
12.	13.0	12.7	12.6	11.9	12.0	11.3
Q.	35.10	34.50	34.50	33.50	33.30	32.20

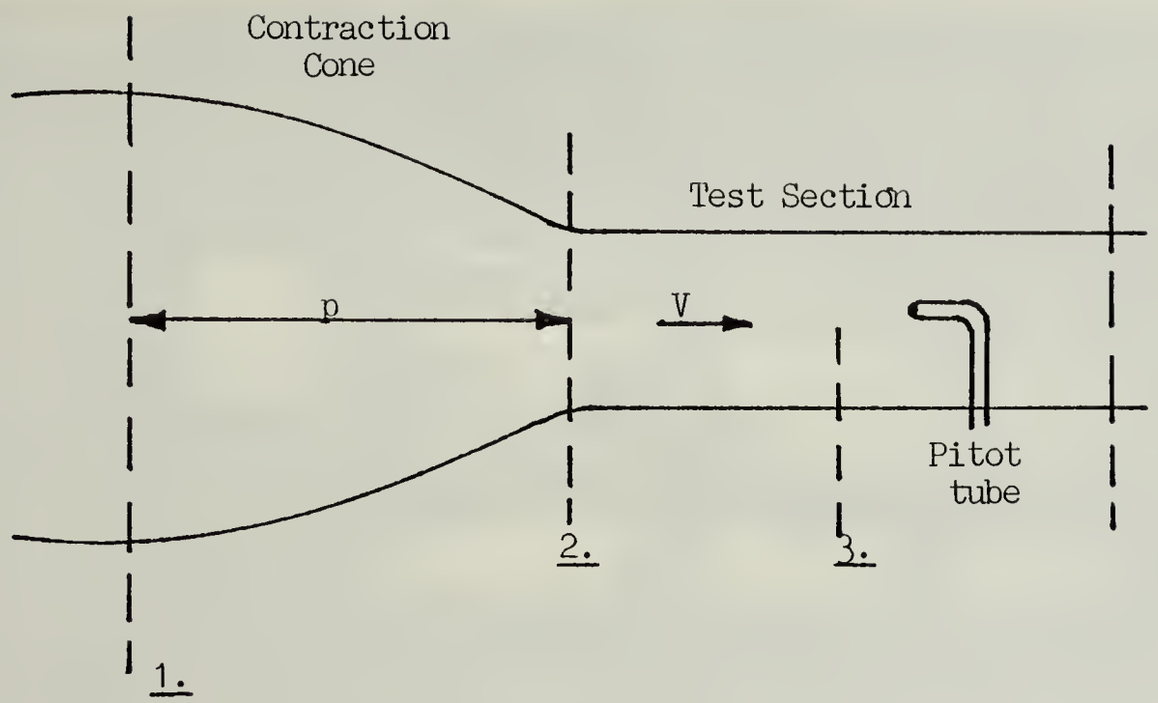

FIGURE 39. Test Section Flow

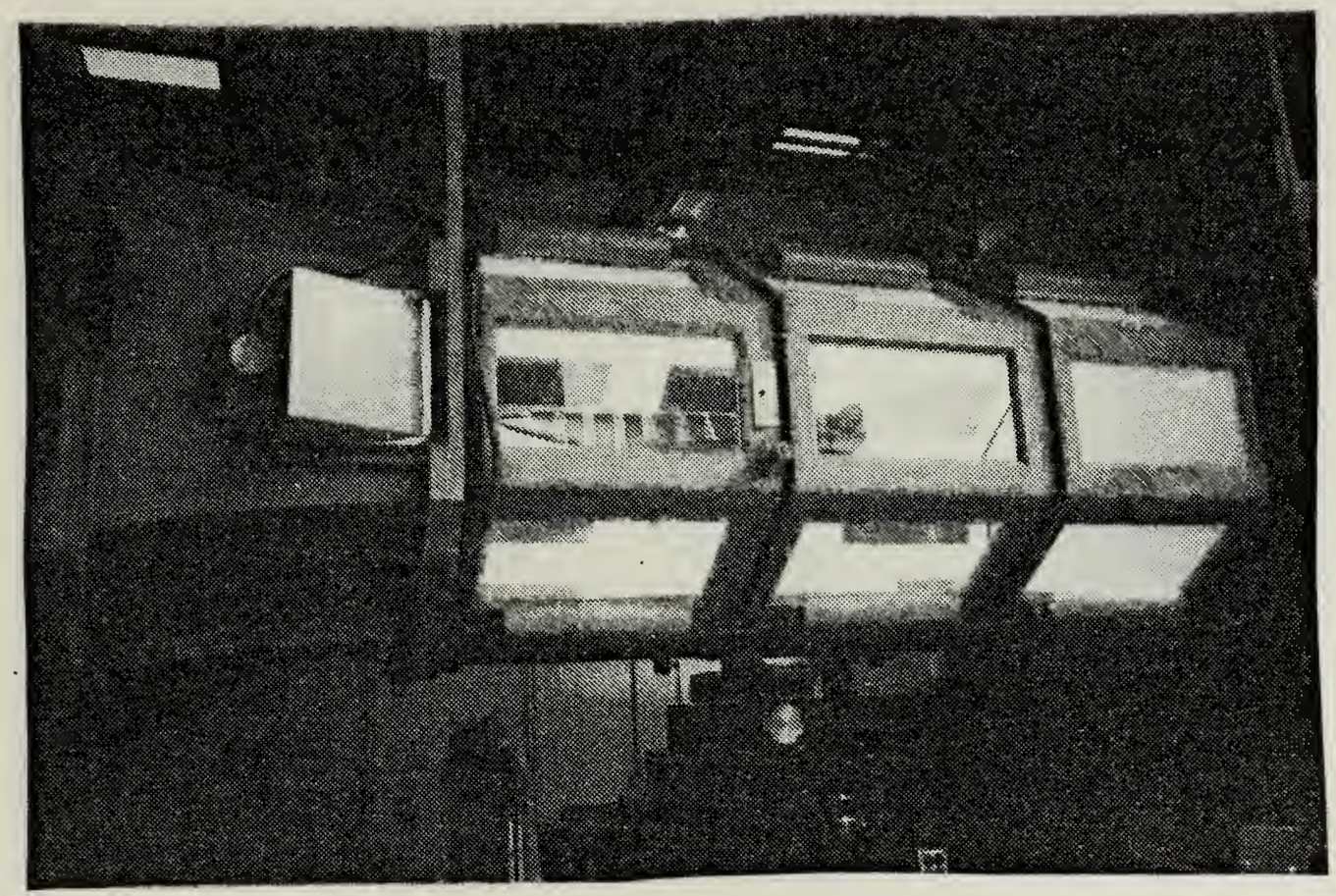

FIGURE 40. Test Section

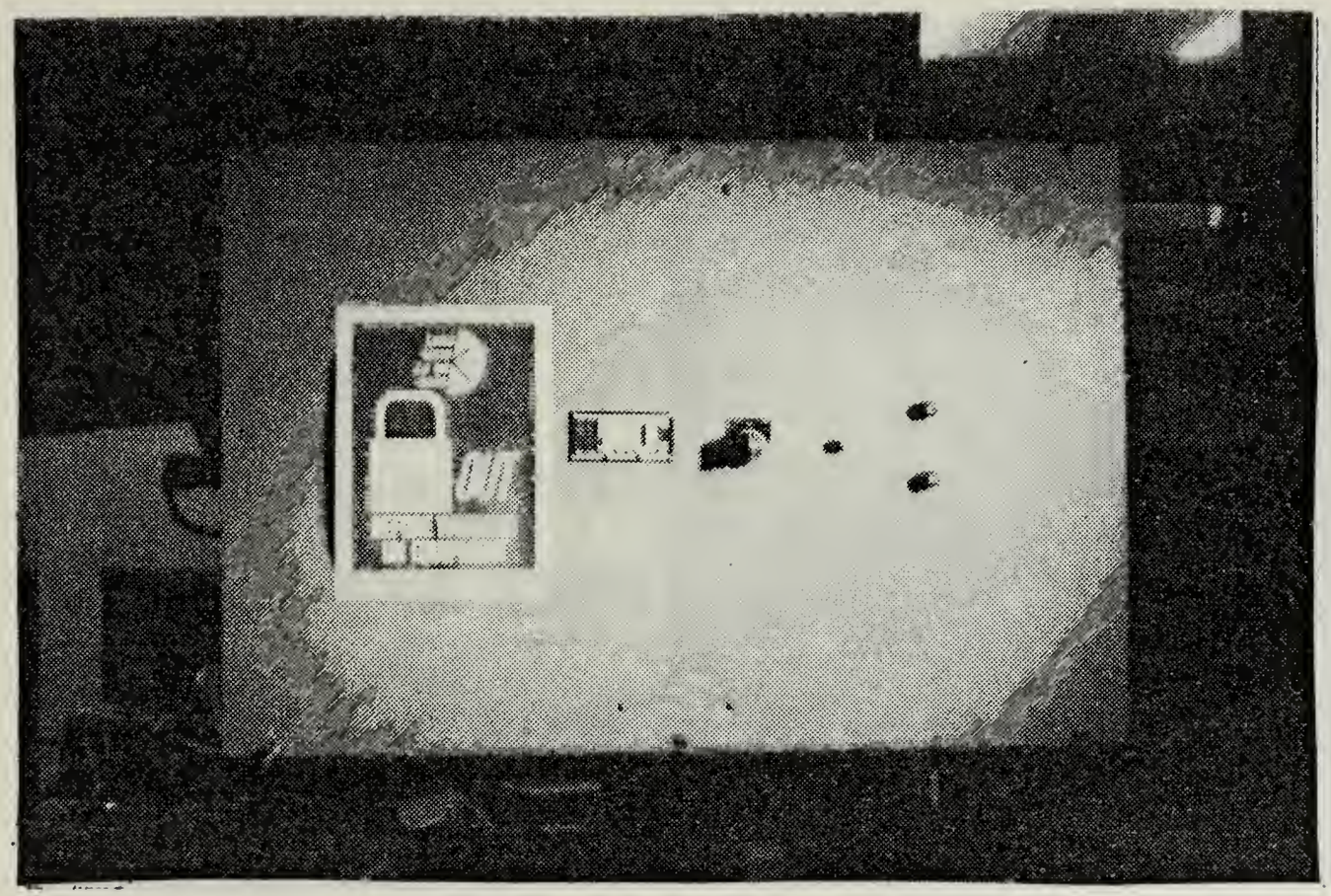

FIGURE 41. Power Panel

FIGURE 42. Control Panel

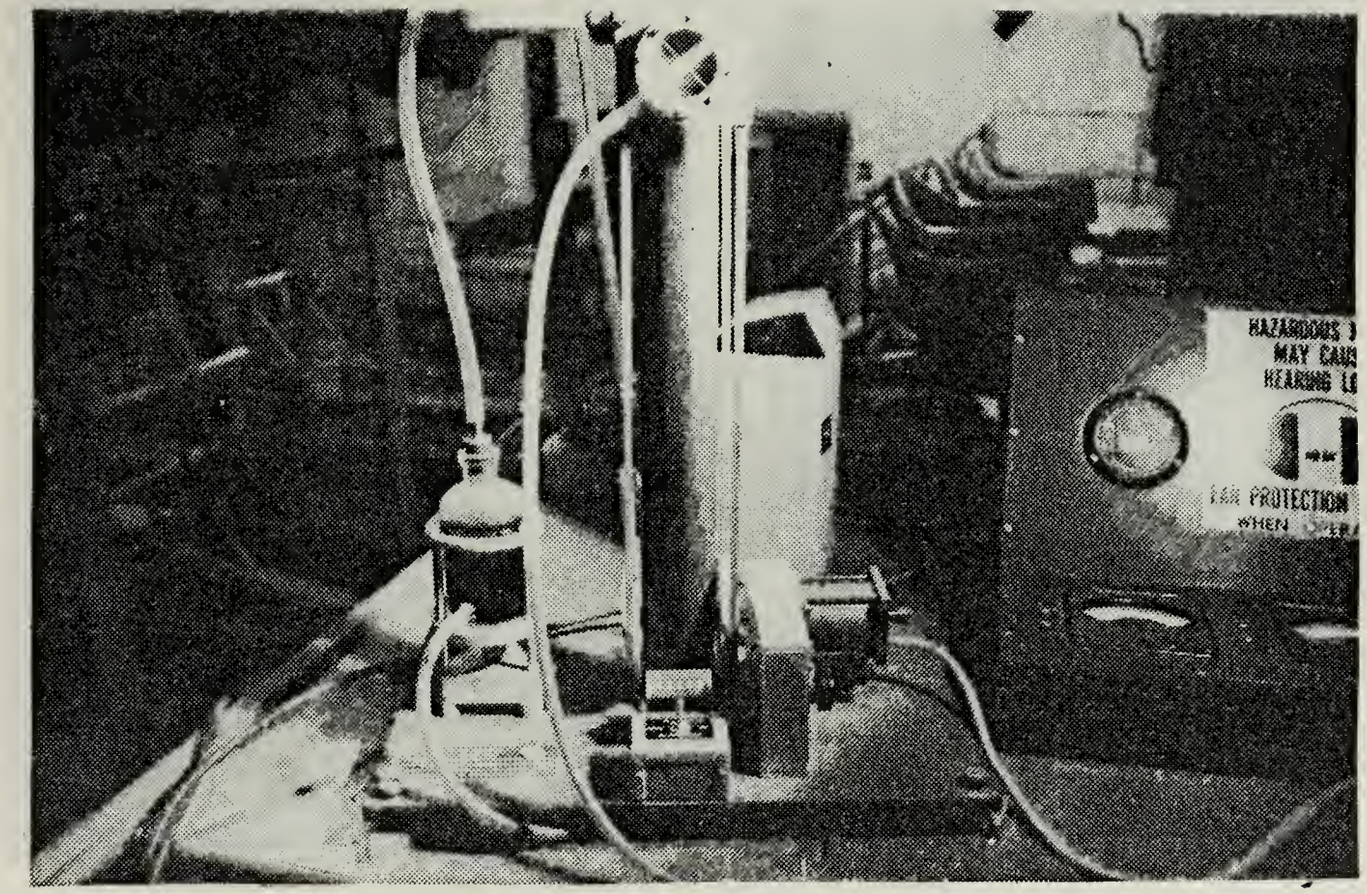

FIGURE 43. U-tube Manometer

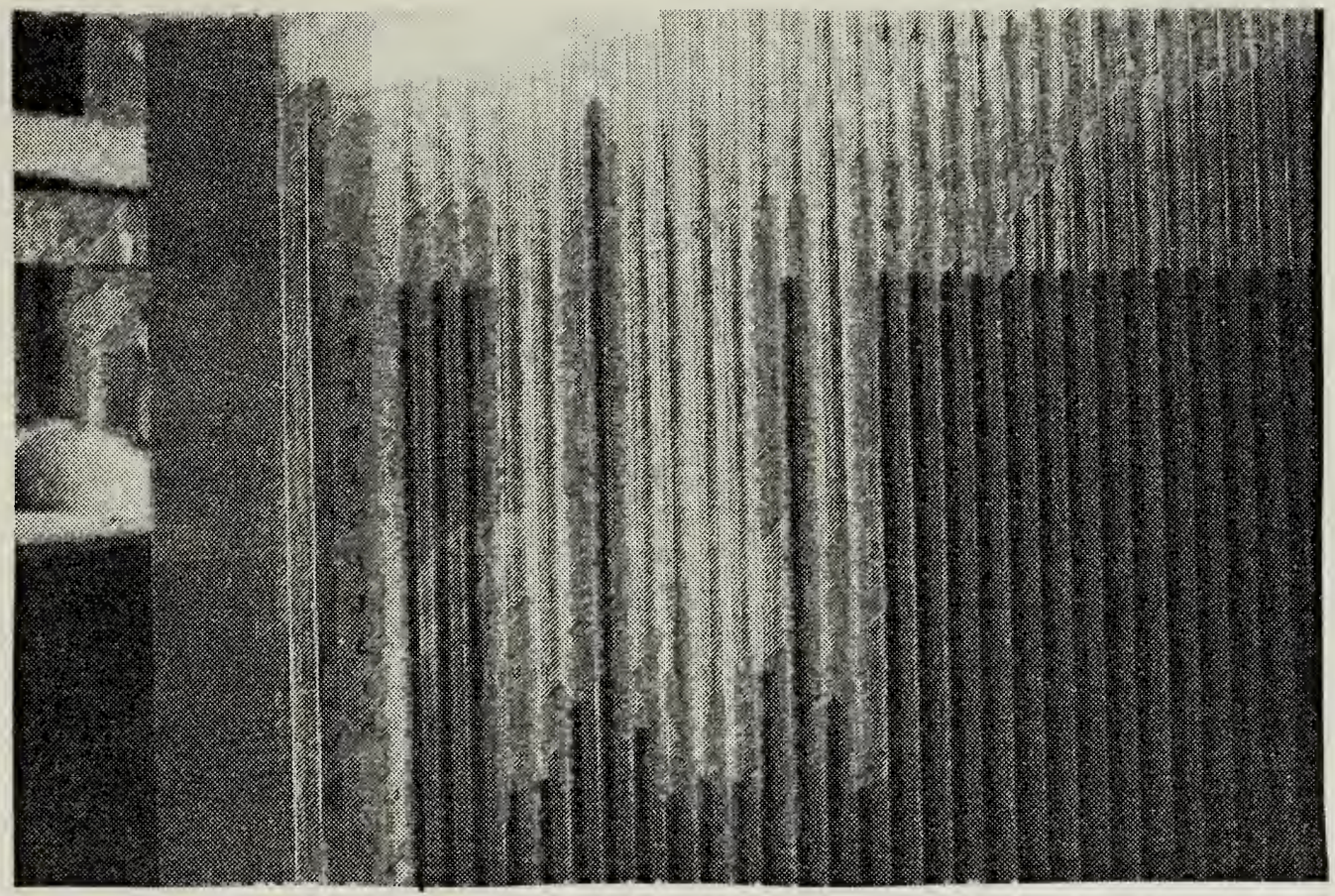

FIGURE 44. Flow Anomaly

BIBLIOGRAPHY

Gorlin, S. M. and Slezinger, I. I., Wind Tunnels and their Instrumentation, Israel Program for Scientific Translations, 1964.

Pope, A. and Harper, J. J., Low Speed Windtunnel Testing, Wiley, 1966.

Robinson, R. F. and Novak, D. H., Introduction to Wind Tunnel Testing, Shaw, 1952.

LIST OF REFERENCES

1. McDonnell Aircraft Company, RF/A-18A Nose Shape (Lower Mold Line), paper presented to Naval Air Development Center, Warminster, Pennsylvania, 12 August 1981.

2. Ibid.

3. Ibid.

4. Naval Air Systems Command Operations Report 0873 TW, Photographic Reconnaissance Requirement for the RF/A-18 Aircraft, 1 August 1973.

5. McDonnell Aircraft Company, RF/A-18A Nose Shape (Lower Mold Line), paper presented to Naval Air Development Center, Warminster, Pennsylvania, 12 August 1981.

6. Ibid.

7. Ibid.

8. Ibid.

9. Pope, A. Windtunnel Testing, 2d ed., p. 6-9, Wiley, 1954.

10. Ibid., p. 86.

11. Ibid., p. 82

12. Ibid., p. 107

13. Ibid.

14. Ibid., p. 106

15. Ibid.

16. Ibid., p. 80

17. Ibid., p. 84

18. Ibid., p. 105

19. Ibid., p. 106

INITIAL DISTRIBUTION LIST

		No. Copies
1.	Defense Technical Information Center Cameron Station Alexandria, Virginia 22314	2
2.	Library Code 0142 Naval Postgraduate School Monterey, Ca 93940	2
3.	Commanding Officer Naval Air Development Center Warminster, Pennsylvania 18974	5
4.	LT. Joseph W. Poole 177 Webster Street #220 Monterey, Ca 93940	10
5.	Harvey W. Burden, Code 67Zx Naval Postgraduate School Monterey, Ca. 93940	5
6.	Donald M Layton, Code 67Ln Naval Postgraduate School Monterey, Ca 93940	2
7.	Lynn Von Geldern P. O. Box 334 Monterey, Ca 93940	1

202202
Thesis
P739
c.1
Poole
An experimental investigation into the forebody and engine inlet airflow characteristics of a photographic reconnaissance window pallet on the RF/A-18 aircraft.